https://doi.org/10.15407/ufm.27.03.445

V.Yu. DANILCHENKO*, V.I. BONDAR, and Ye.M. DZEVIN*****
G.V. Kurdyumov Institute for Metal Physics of the N.A.S. of Ukraine,
36 Acad. Vernadsky Blvd., 03142 Kyiv, Ukraine

* danila@imp.kiev.ua,** vib@imp.kiev.ua, *** dzevin@i.ua

LASER-STIMULATED STRUCTURAL AND PHASE TRANSFORMATIONS IN NEAR-SURFACE LAYERS OF IRON-BASED ALLOYS

The results of studies concerning the formation of the structural state of single crystals and polycrystals of iron and its alloys under sharply unbalanced conditions of pulsed laser treatment are reviewed and analysed. As shown, significant heating–cooling rates during laser treatment result in a decrease in the temperature of the γ–α-transformation and in the formation of the γ-phase. In this case, recrystallization of single crystals of α-iron is observed, as a result of which, a polycrystalline component of α-iron is formed with a b.c.c.-lattice parameter that corresponds to the initial one and, during remelting in a narrow range of energy densities, a single-crystal region of the γ-phase with an increased f.c.c.-lattice parameter and significant texture is for-med too. As established, the mechanical properties along the depth of the laser influence zone are determined mainly by structural factors and change according to nonmonotonic curves with a maximum. The influence of energy parameters of pulsed laser irradiation on the formation of wavy microgeometry of the surface is revealed.

Keywords: laser treatment, single crystal of α-iron, structure, austenite, martensite, residual stresses.

Citation: V.Yu. Danilchenko, V.I. Bondar, and Ye.M. Dzevin, Laser-Stimulated Structural and Phase Transformations in Near-Surface Layers of Iron-Based Alloys, *Progress in Physics of Metals*, **27**, No. 3: 447–495 (2026)

1. Introduction

Laser treatment (LT) is used in almost all industries. In the last 15–20 years, the intensive development of modern electronics, the development of materials for medical purposes and functional materials have put forward increased requirements for LT technology [1–5]. The ever-increasing requirements of the industry have led to the need for a more complete use of the reserves of LT [6–10]. This can be achieved only with purposeful control of the parameters of structural and phase transformations that occur during laser heating and subsequent cooling.

The development of LT technology and its wide application in industry requires an in-depth study of the regularities of physical processes during LT, the development of adequate models that take into account all the diversity of the structural and phase state of alloys that were formed under conditions of ultrafast heating. The structural state of steels formed with the help of continuous LT has been studied quite fully; however, the features of structural and phase transformations under sharply nonequilibrium conditions of pulsed LT have remained insufficiently studied. This situation complicates the establishment of a relationship between the parameters of LT and the complex of physical-and-mechanical characteristics of local areas of processed alloys. With pulsed LT, the temperature gradient in the surface layer of 100–150 μm thick is up to 10^6 °C/cm, and the heating and subsequent cooling rates are of 10^5–10^8 °C/s and 10^4–10^6 °C/s, respectively. The latter far exceeds the critical cooling rates sufficient for quenching under normal heating conditions. As a result, highly dispersed structural components with a high content of crystal structure defects and a specific distribution of alloying elements are formed in the surface layers [11–14].

X-ray diffraction studies of steels after LT were traditionally carried out on polycrystalline samples, which made it possible to reveal the most significant changes in the structural and phase state. With the low sensitivity of the polycrystalline method, subtle structural effects remained unexplored. The need to study subtle structural changes and the behaviour of individual substructural components in steel requires the use of single-crystal samples. X-ray diffraction of single crystals makes it possible to observe subtle diffraction effects, measure small amounts of phase components, and investigate crystallographic orientation aspects of the structural state.

Due to the high temperature gradient and cooling rate during pulsed LT, a specific structural state is formed with a special distribution of residual stresses, which is determined by both thermal processes and structural changes in the surface layers. The need to study the nature of residual stresses is associated with their ability to activate or slow down phase and structural changes, act as a strengthening or weakening fac-

tor, which is especially important for parts that operate under cyclic variable loadings.

This review analyses the experimental results of studying the influence of pulsed LT regimes on structural and phase transformations and the structural and stressed state of iron-based metastable alloys.

An analysis of the results of studies of the formation of the structural state of single crystals and polycrystals of iron and iron-based alloys under sharply nonequilibrium conditions of pulsed laser treatment is made. As shown, a significant heating–cooling rate during laser treatment leads to a decrease in the temperature of the γ–α-transformation and formation of the γ-phase. In this case, the recrystallization of single crystals of α-iron is observed, as a result of which a polycrystalline component of α-iron is formed with a b.c.c.-lattice parameter that corresponds to the initial one, and, during melting in a narrow range of energy densities, a single-crystal region of the γ-phase with an increased f.c.c.-lattice parameter and significant texture is formed too. It has been established that the mechanical properties with respect to the depth of the laser effect zone are determined mainly by structural factors and vary along nonmonotonic curves with a maximum. The influence of the energy parameters of pulsed LT on the formation of wavy surface microgeometry is revealed. The dependence of the nature of residual stresses on the regimes of LT on carbon steels is described.

2. Recrystallization of α-Fe Single Crystals Stimulated by LT

During the formation of the structural state of iron under sharply nonequilibrium conditions of rapid cooling, there is a tendency to lower the temperature of the γ–α-transformation and the formation of the γ-phase. In iron alloys, as a result of heating in the γ-region and subsequent cooling to room temperature, polymorphic transformations occur, which can be realised both by a crystallographically ordered and disordered mechanism. Rapid cooling can retard the disordered diffusive displacements of atoms. Therefore, depending on the rate of heating and cooling, the contribution of each of these mechanisms can vary significantly [15–20].

In technically pure iron, by rapid cooling, it was possible to reduce the temperature of the γ–α-transformation and implement it according to the martensitic mechanism [21]. In the process of iron cooling at different rates, this transformation was stepwise, and the lowest temperature step of the γ–α-transformation, accompanied by the formation of a characteristic relief, was fixed at 420 °C [21].

In works [17, 19, 22–24], the effect of pulsed LT on the structural and phase state and the change in the parameters of martensitic transformations in iron alloys was studied.

The x-ray photo method of single-crystal samples is more reliable and informative than the traditional polycrystal method. It allows observing small amounts of phases and subtle diffraction effects that are not complicated by the influence of interphase boundaries. These effects can reflect the orientation aspects of γ–α- and α–γ-transformations, in particular, the degree of crystal lattice fragmentation, the crystallographic relationship between the lattices of the transforming phases, the transformation texture, *etc*.

LT of single-crystal samples was carried out in an air atmosphere using QWANT-18 M equipment by pulses with duration of 8 ms. During laser treatment of massive ingots, the subsequent cutting of cylindrical samples for x-ray studies inevitably led to the need to remove the hardened layer, comparable in thickness to the layer treated by the laser beam. Under such conditions, it was not possible to achieve the full effect of autoquenching by ultrafast cooling at a rate of 10^5–10^6 °C/s. The energy of the laser beam was successively increased from 5 J to 15 J. In this case, the regime was provided from heating in the γ-region without melting (0.5–3 J/mm^2) to premelting (3–6 J/mm^2), melting (6.5–18 J/mm^2) and melting of the surface almost to the centre of the sample (18–25 J/mm^2). In the latter case, a welding nozzle was used. X-ray investigation was made after each laser treatment. The crystal lattice parameters were determined from the position of diffraction reflections relative to the lines of the standard. At room temperature, using the pole figure of b.c.c. iron, the intervals of sample rocking angles corresponding to certain diffraction reflections were found. The saturation magnetisation of iron samples was studied by the magnetometric method in a differential magnetometer.

Studies of single-crystal samples of austenitic alloys with an f.c.c. lattice showed that LT did not cause their recrystallization. In this case, the reflections of the γ-phase turned out to be more diffuse in the azimuthal direction, which indicated a misorientation of the austenite fragments. An increase of the energy density of laser radiation led to an increase of the angle of maximum misorientation of the austenite lattice. In this case, the crystal lattice parameters of the binary N3O alloy (Fe–0.02 C–30 Ni, wt.%) did not change, while the parameters of the 180N5 carbon alloy (Fe–1.8 C–5 Ni, wt.%) slightly increased due to the dissolution of graphite globules in it. LT in the premelting mode led to the formation of a large number of γ-grains orientationally unrelated to the initial γ-phase.

Thus, the LT of alloys with the f.c.c. lattice did not lead to significant structural changes, and studies were continued on single crystals of metals with the b.c.c. lattice.

Single crystals of Armco and siliceous α-iron were used as objects of study. X-ray rotation diffraction patterns of the initial single crystals, as well as diffraction patterns from a stationary sample, the position of which changed successively after 2° in the range of angles of 45°, had the

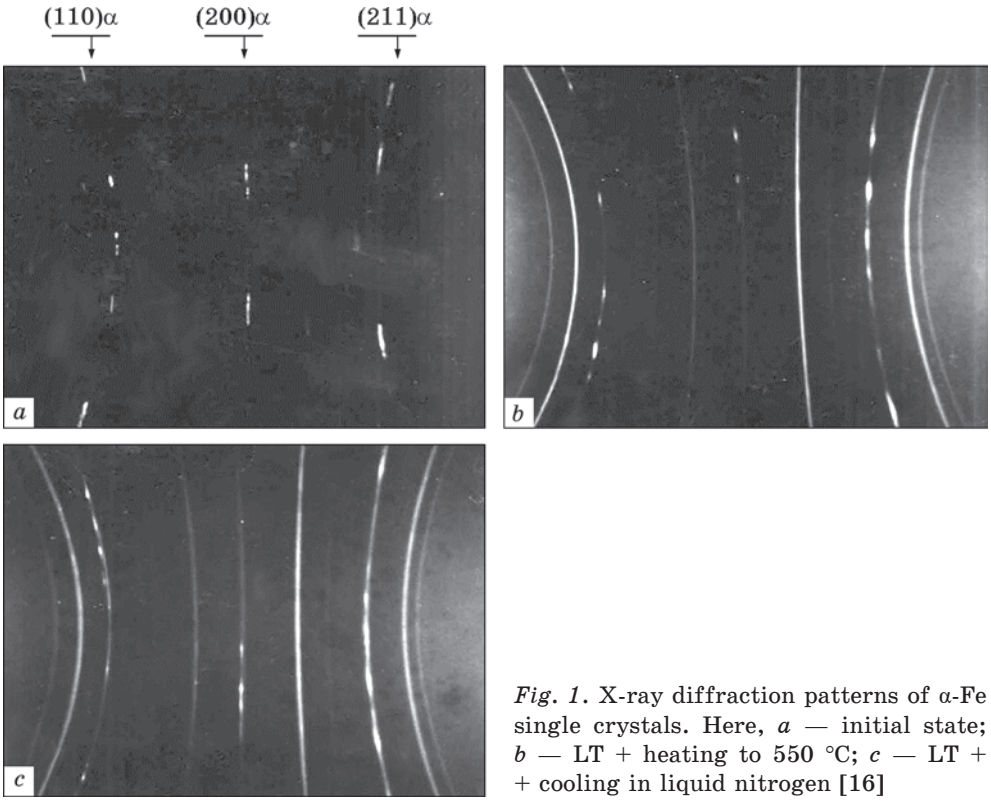

Fig. 1. X-ray diffraction patterns of α-Fe single crystals. Here, *a* — initial state; *b* — LT + heating to 550 °C; *c* — LT + + cooling in liquid nitrogen [16]

diffraction reflections only from the b.c.c. lattice (Fig. 1, *a*). The lattice parameter a_α of Armco-iron single crystal turned out to be equal to 0.2866–0.0001 nm, and that of a silicon iron crystal to be equal to 0.2864–0.0001 nm. The reduced value of a_α in the latter case is associated with the presence of silicon in the α-solid solution [25].

The regularities of the formation of the structural state during laser heating and subsequent recrystallization of single crystals turned out to be similar for Armco and silicon iron. Therefore, in the following, the characteristics of the structure of single crystals are given mainly for Armco iron.

A further increase in the energy of the laser beam did not change the diffraction pattern, but heating in the melting mode led to significant changes in the diffraction pattern and, accordingly, in the structural state of the initial α-iron single crystal. Rapid cooling of the surface layer of the sample from the liquid state led to the formation of polycrystalline α-iron with a b.c.c. lattice having a crystal lattice parameter coinciding with the lattice parameter of the original sample [17]. This was evident from the formation of continuous Debye lines of α-iron passing through all diffraction reflections from the initial single crystal. In this case, the recrys-

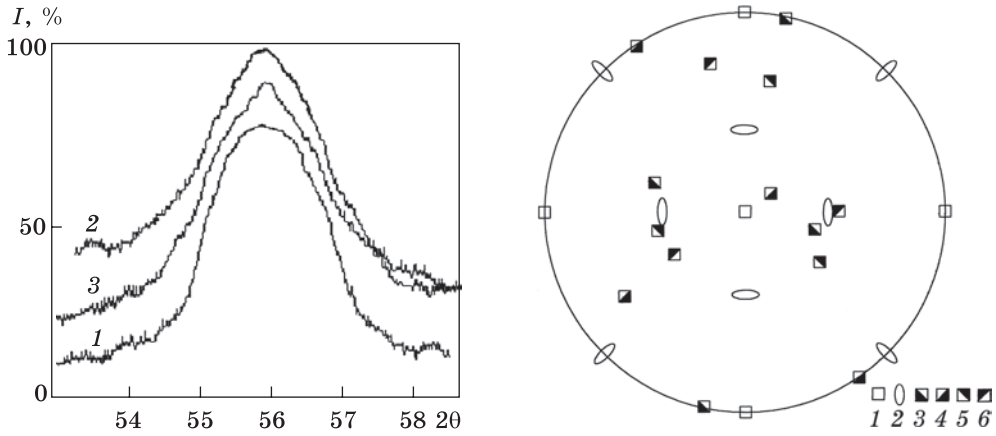

Fig. 2. Microphotometer curves of the x-ray $(211)_\alpha$ reflexes: initial single crystal (*1*), $\{211\}_\alpha$ single- (*2*) and polycrystalline (*3*) components of α-phase after LT of 16 J/mm² energy density [53]

Fig. 3. Pole figure of a single crystal of Armco iron after LT (22 J/mm² energy density): *1*, *2* — $(200)_\alpha$, $(220)_\alpha$ initial single crystal of α-iron; *3*–6 — $(200)_\gamma$ γ-phase with a relative intensity of 100, 40, 25, and 10% [16]

tallization of the surface layer did not occur completely. The reflections from the initial single crystal did not change their angular position on the x-ray pattern, which indicated that the crystallographic orientation of the lattice of a certain volume fraction was retained during crystallisation.

Figure 2 shows the shape of diffraction reflections in the form of microphotometric curves. It can be seen that the half-width of the reflections from the polycrystalline component of the α-phase increased in comparison with the reflection from the lattice of the initial single crystal. The half-width of reflections from the single-crystal region of the α-phase increased further, since such reflections were superimposed by solid Debye lines from the polycrystalline α-phase. An increase in the half-width of reflections indicated an increase in the density of dislocations in the melted layer, which appeared, when shock waves appeared during laser heating, as well as due to phase hardening.

Comparison of the intensity (according to microphotometric curves) of individual reflections from the α-phase and solid Debye lines with the same Miller indices shows that in the surface layer after melting, the proportion of the polycrystalline component of the α-phase was 10–80% at an energy density of 12–24.5 J/mm².

A qualitative change in the diffraction pattern was observed when the energy density reached 12–14 J/mm². In this case, the γ-phase was additionally recorded, the reflections from which had the form of reflections from single-crystal grains (Fig. 1, *b*). The polycrystalline component of the

γ-phase was not observed under any laser treatment regimes. In various experiments, from two variants to four ones of the lattice orientations of the γ-phase relative to the lattice of the initial single crystal with a b.c.c. lattice were fixed. The intensity of reflections $(200)_\gamma$ from lattices of different orientations differed significantly, and this difference was by 2–5 times (Fig. 3). The misorientation angle φ_γ of the lattice of the γ-phase was equal to 1.6–2.6°, which is significantly less than for the α-phase. For orientations of lattices formed in a smaller amount, the angle φ_γ somewhat decreased. In this case, the intensity of the γ-phase reflections for the silicon iron was higher compared to technical iron at the same energy density of the laser beam. In some experiments, the excess of the intensity, for example, of the $(200)_\gamma$ reflex reached 8–10%. This was caused by an additional decrease in the critical temperature of the α–γ-transformation (along with a high cooling rate and the possible dissolution of nitrogen from the atmosphere in the molten bath) and, as a result, the formation of an additional amount of overcooled austenite when alloying the solid solution with silicon. In addition, the effect of an increase in the intensity of the $(200)_\gamma$ reflection, apparently, can also be associated with an increase in the texture mismatch in the diffraction pattern.

Laser melting at high energy densities (above 20 J/mm^2) no longer led to the formation of the γ-phase. Therefore, the formation of γ-iron was observed during LT in a certain range of energy density (from 12 to 18 J/mm^2). Similarly to this dependence, it was previously shown [25, 26] that in iron powders obtained by rapid cooling from a liquid state, the f.c.c. phase of iron was formed in a narrow range of cooling rates of 10^5–10^6 °C/s at particle sizes of 30–280 μm. A further increase in the cooling rate caused the formation of only the b.c.c. phase in iron powders, similarly to how, in our experiments, laser heating with an energy density above 20 J/mm^2 again led to the formation of a b.c.c. structure in the surface layer. Such a rule in the change of the structure of iron from b.c.c. to f.c.c. and again to b.c.c. lattice with an increase in the cooling rate above a certain critical value both after laser heating and during ultrafast quenching from a liquid state [26] may indicate the implementation of an incomplete γ–α-transformation, and then fixing the δ-phase.

An analysis of changes in the diffraction pattern and the magnitude of the crystal lattice parameters of the phase components makes it possible to present the mechanism of structure formation of technical iron after laser treatment as follows.

As a result of crystallisation after laser melting, grains of the γ-phase were formed, which, upon further cooling at the point of the γ–α-transformation, completely recrystallized into a polycrystalline aggregate of the α-phase. It can be assumed that those regions of the γ-phase were recrystallized, in which the dissolution of interstitial impurities from atmospheric air did not take place. This is evidenced by the fact that the

crystal lattice parameter of the α-phase is equal in the original sample and after laser melting. The local regions of the γ-phase, in which the dissolution of impurities from the atmosphere occurred, had a significantly lower point of the γ–α-transformation, did not undergo the indicated recrystallization, which made it possible to observe γ-reflections on x-ray patterns in the form of reflections from single-crystal regions with an f.c.c. lattice.

In addition to the impurity factor, one should also take into account the possibility of the dislocation factor of lowering the γ–α-transformation point. In Ref. [27], the possibility of martensitic transformation through an intermediate hexagonal close-packed phase was studied. As a consequence of such a rearrangement, it was indicated that there are a large number of dislocations and packing defects in the newly formed γ-phase, which significantly inhibit the possibility of recrystallization processes immediately after the phase transformation. During high-speed cooling in the LT process, the appearance of newly formed dislocations will slow down the removal of phase hardening and the possibility of dislocation creeping of the α-phase. Consequently, some volume of the γ-phase with a defect structure may turn out to be stabilised from being able to complete the phase transformation. In Ref. [27], it was noted that, regardless of the carbon content in the steel, the first portions of the formed γ-phase have a composition close to eutectoid (with 0.7–0.8% C).

The b.c.c. lattice parameter for all laser treatment modes turned out to be practically the same for single- and polycrystalline components of the α-phase. The fact of an increase in the amount of the polycrystalline component of b.c.c. iron under regimes when the regions of f.c.c. iron were not detected by x-ray diffraction suggests that the α-phase was formed mainly in the form of a single-crystal component with an orientation coinciding with the initial orientation of the single crystal, and δ-phase in the form of a polycrystalline component.

For comparison, it should be noted that the quenching of iron in organic liquids led to the formation of α- and γ-solid solutions with an increased parameter of their lattices, and when quenched in water, the parameters of b.c.c. and f.c.c. lattices had values corresponding to the state of α- and γ-iron without introduced implementations; when quenched in ethanol, the iron powder contained up to 1.5 wt.% carbon and 0.5 wt.% oxygen [26]. In Ref. [26], carbide Fe_2C and wüstite FeO, which were formed as a result of the developed active surface of dispersed iron particles, were fixed as accompanying phases. In our experiments, these phases were not observed due to the much smaller active surface of the layer heated by the laser beam.

The γ-Fe was also detected in electroerosive iron powders [28], in ultrafine powders as products of plasma-chemical reactions of pyrolysis of iron carbonyls at a high-voltage discharge [29], in iron films grown on a substrate of other metals [30–34], in the volume of amorphous films [30] or during their subsequent crystallization [35] after forced nitrocarburi-

zing in propane-butane-nitrogen [36]. Consequently, the tendency to the formation of the γ-phase manifests itself during the formation of the structural state of iron under certain nonequilibrium conditions (high heating and cooling rates, dispersed powders, thin films, surface layers, *etc*.).

The maximum misorientation angle φ_α, which characterises the degree of fragmentation of the b.c.c. lattice, was determined from the azimuthal smearing of the reflections $(200)_\alpha$ and $(211)_\alpha$ according to the formula [37]:

$$\varphi = 2\arcsin\sqrt{\frac{a^2 - (b-c)^2}{4bc}}, \qquad (1)$$

where a is the length of the x-ray spot in azimuth;

$$b = \sqrt{h_1^{\,2} + r^2}; \quad c = \sqrt{h_2^{\,2} + r^2};$$

h_1 and h_2 are the distances from the beginning and end of the spot to the equator of the x-ray film, respectively; r is the x-ray camera radius.

In the initial state, the angle φ_α was equal to 1.8° for an Armco iron single crystal. Laser pulse heating by 5–20 J/mm^2 led to some increasing of φ_α and practically did not change the parameters of the b.c.c. lattice.

X-ray investigations of the sample after chemical etching showed that reflections from a single crystal of the initial orientation were formed at a depth less than the penetration depth of x-rays. For the radiation of an iron anode in the study of alloys based on iron, this depth is about 10 μm. This means that the formation of reflections of the initial orientation is associated not only with reflection from the layers of the sample located under the melted layer. But also, apparently, from layers formed as a result of a partial epitaxial effect of melt crystallisation on an oriented single-crystal substrate, which was the unmelted part of the sample.

Indeed, at the stage of crystallisation of the laser melting zone, the grains of the unmelted substrate can affect the growth of crystals during solidification of the liquid bath as effective nuclei. In particular, the influence of the grain size of the unmelted substrate on the grain size formed during the solidification of the laser melting zone in chromium steel and technical iron was found [38], and it was also shown that unmelted grains can serve as the beginning of the growth of dendritic crystals in the melting zone [39].

The φ_α angle after melting turned out to be much larger than for the original single crystal, and amounted to 3–4°. Such a change in the structural state of the α-phase was not associated with a change in its chemical composition, since the parameter a_α did not change after laser melting. An increase of the φ_α angle in the surface layer was associated with significant internal stresses arising during rapid crystallisation, as well as with a decrease in the driving force of epitaxial crystallisation.

When analysing the diffraction pattern of the γ-phase lattice, a significant textural discrepancy between the intensity of reflections draws

attention. The intensity of the $(200)_\gamma$ reflection during laser melting sharply increased relative to the $(111)_\gamma$ reflection. The intensity ratio $I_{(200)\gamma}/I_{(111)\gamma}$ for the untextured f.c.c. phase is of 0.64 [40]. Such a discrepancy is usually observed in the dendritic structure of the sample, which is characteristic of rapid cooling of the molten metal. A microstructure study showed that after laser melting, the samples indeed have a dendritic structure. This regularity was noted in the literature earlier [41, 42]. In the zone of laser melting, *e.g.*, AISI 52100 steel, a well-pronounced dendritic structure was observed, for which there was a textural discrepancy between the intensity of x-ray reflections: the intensity of the $(200)_\gamma$ line relative to the $(111)_\gamma$ line increased by 7–8 times, when passing through the melting threshold [42]. In our experiments with technical iron, a significantly higher ratio of the intensity of these reflections was achieved: 10 times or more. When melted by a laser beam with an energy density of 14–18 J/mm^2, at a sufficiently high intensity of the $(200)_\gamma$ reflex, only traces of the $(111)_\gamma$ reflections were recorded, and for some orientations of the γ-phase, the latter reflections were not observed. In this regard, the determination of the amount of residual austenite in iron-based alloys after laser melting can be correctly carried out only by a pair of lines $(111)_\gamma$–$(110)_\alpha$, which is included in the Kurdjumov–Sachs orientation relation between the austenite and martensite lattices. This relation is fulfilled in steel that has been subjected to laser remelting [43]. This possibility remains since during the γ–α-transformation the $(111)_\gamma$ plane remains parallel to the $(110)_\alpha$ plane, which means that the intensity ratio of the corresponding x-ray reflections is preserved. For any other pairs of reflections, this is not the case, and the amount of residual austenite determined from the ratio of their intensity may differ from the actual one by several times.

3. The Change of the γ-Phase Crystal Structure as a Result of Laser Melting

Changes in the crystal structure of austenite and the possibility of dissolution of introduced atoms in it as a result of high-energy processing of Fe-based alloys were studied in works [44–53].

The parameter a_γ of γ-phase of the Armco iron after laser melting was of 0.3593 nm that is significantly higher than the value obtained by extrapolating the austenite lattice parameter to zero concentration of interstitial atoms. It should be noted that the last value of the parameter turns out to be different, when extrapolated to zero concentrations of carbon (0.3556 nm) and nitrogen (0.3566 nm) [44, 45]. For comparison, we point out that the parameter a_α of the α-Fe phase, obtained by extrapolating the martensitic lattice parameter to zero concentration of both carbon and nitrogen, turns out to be equal to 0.2866 nm [44].

The increased a_γ value was associated with the dissolution of nitrogen and carbon atoms from the atmosphere in the iron melt during its laser melting. This possibility has been repeatedly noted in the literature [45–47]. In addition, during electric-arc processes (melting in arc furnaces, welding), an intensive absorption of nitrogen from atmospheric air by liquid metal was observed [48]. In Ref. [49], based on the analysis of the chemical composition of the metal after plasma remelting, it was concluded that using plasma, nitrogen can be introduced into the metal in an amount significantly exceeding the equilibrium for ordinary melting conditions at the same partial pressure of nitrogen in the gas phase. In this case, the plasma is presented as a kind of pump for pumping nitrogen into the melt. Similarly, during LT, gas breakdown and the formation of a plasma cloud in the irradiation zone can occur. As a result of the interaction of plasma with the surface (molten metal), the chemical composition of the surface layers changes and nitriding or cementation takes place. Therefore, this type of treatment is also called laser–plasma synthesis. As is known, during laser–plasma synthesis, during the action of a laser pulse, the material being processed is heated with the formation of a plasma torch near the surface. Due to the ambivalent diffusion of particles from the plasma volume, the treated surface is charged negatively to a potential of 4–6 V. The appearance of a negative potential, therefore, causes an accelerated movement of ions to the sample surface.

It is necessary to take into account the possibility of the absorption of carbon by the molten metal as well (with the predominant absorption of nitrogen). In this case, in the presence of carbon, the solubility of nitrogen can increase sharply, as was the case, *e.g.*, in arc processes [49].

The nitrogen content in the γ-Fe solid solution can be estimated according to Ref. [54] using the formula

$$a_\gamma = 0.3566 + 0.0008C_N, \quad (2)$$

and the carbon content can be estimated according to the formula

$$a_\gamma = 0.3556 + 0.00095C_C, \quad (3)$$

where C_N and C_C are the atomic concentrations of nitrogen and carbon, respectively.

It can be seen that the dependences of a_γ on the content of nitrogen and carbon are very close; however, as noted above, extrapolation of a_γ to zero concentration of nitrogen and carbon gives different values of the pure iron parameter. The difference between these values is 0.001 nm, which is much higher than the accuracy of measuring the crystal lattice parameter.

If we assume that the value of a_γ is determined mainly by the saturation of the solid solution by nitrogen, then its content can reach 0.862 wt.%. In the case of dissolution of carbon in γ-iron, its content turns out to be close (0.864 wt.%). In fact, in γ-Fe, apparently, both C was

dissolved during the dissolution of cementite particles, and N was dissolved during the formation of plasma from atmospheric air. Therefore, it could be considered that the value of 0.86 wt.% corresponds to the total content of nitrogen and carbon in γ-solid solution.

However, the total content of nitrogen and carbon in γ-iron may, apparently, turn out to be overestimated, since the expressions given above are valid for a massive sample, as noted in Ref. [51], and in our case we are talking about dispersed particles of the γ-phase with a small volume fraction (2–3%) distributed in α-iron. Its dispersivity and high level of internal stresses can significantly change the conditions of nitrogen dissolution in it. In addition, it should be taken into account that during pulsed laser heating, a significant heating of the metal bath takes place and a high-pressure zone up to 10^6–10^7 Pa [54] appears, in which the dissolution of nitrogen can be facilitated.

However, the total content of nitrogen and carbon in γ-iron may turn out to be overestimated, since the given expressions are valid for a massive sample, and work [51] refers to dispersed particles of the γ-phase with a small volume fraction (5–7%), distributed in α-iron. Their dispersion and high level of internal stresses can significantly change the conditions of nitrogen dissolution. In addition, it is necessary to take into account that during pulsed laser heating, a significant heating of the metal bath takes place and a high-pressure zone up to 10^6–10^7 Pa [54] occurs, in which the dissolution of nitrogen can be facilitated.

The a_α parameter in the initial state and after LT was practically the same. It means that, in the b.c.c. iron, the atmospheric nitrogen practically did not dissolve. From the fact of the increased parameter a_γ, we can conclude that the γ-phase was formed not due to overcooling of iron from the γ-region, but due to a decrease in the temperature of completion of the γ–α-transformation below room temperature due to saturation of the γ-solid solution with atmospheric nitrogen.

In Ref. [35], it was reported that it is possible to obtain γ-iron of an amorphous ribbon by rapidly cooling the liquid melt from a temperature of 1390 °C, and the parameter of the obtained γ-phase, equal to 0.3559 nm, is close to the parameter of austenite at room temperature. However, the cooling rates in this case were significantly lower than those achievable with LT, which affected the significant texture of the γ-phase. The ribbons obtained in a certain range of cooling rates contained both $(111)_\gamma$ and $(200)_\gamma$ reflections, the intensity ratio of which significantly exceeded the tabulated values. Previously, it was established that at cooling rates of 10^5–10^6 °C/s, which are also achievable with LT, the content of residual austenite in technical iron was close to zero [41].

4. The γ–α-Transformation in Armco Fe as a Result of LT

Additional information about the phase and structural state of Armco iron after LT can be obtained by measuring its saturation magnetisation. By cooling to liquid nitrogen temperature and subsequent heating to room temperature, the magnetisation of the initial sample changed almost linearly, and repeated cooling-heating cycles did not change the character of the temperature magnetisation curve (Fig. 4, curve *1*). This indicated the absence of structural changes in the noted temperature range. After that, the sample was melted by a laser beam. The entire surface of the cylindrical sample was treated, including both ends, with laser spots overlapped by 50%. Melting took place almost to the centre of the sample, and thus the sample was remelted by approximately 85–90%. The magnetisation of such a sample turned out to be greater than that of the original one (Fig. 4, curve *2*).

An increase in the magnetisation of Armco iron after laser melting seems to be a complex effect and, apparently, is determined by several factors. In the initial state, the sample contained several (from 3 to 5) crystals of the α-phase with different crystallographic orientations relative to the easy magnetisation axis ⟨100⟩. In such a sample, the total magnetic moment is always less than the value corresponding to the state of magnetic saturation. Indeed, it is known that the isotropy of the magnetic properties of Fe is reduced to the fact that the magnetization of a single crystal with a cubic axis ⟨100⟩ parallel to the direction of an external magnetic field, *e.g.*, with a value of 200 Oe, is of about 1700 G, with an axis along the diagonal of the face ⟨100⟩ is of about 1500 G, and with the axis along the spatial diagonal ⟨100⟩ is of about 1400 G [55]. The formation of a polycrystalline component after laser melting could lead to a texture, in which the easy magnetisation axes of a large number of crystals would be parallel to each other, which, in turn, would lead to the appearance of a magneto-crystallographic preferential direction in the sample. As a result, the saturation magnetisation and, accordingly, the coercive force increase. Similarly, during magnetic-pulse processing of AISI T1, M2

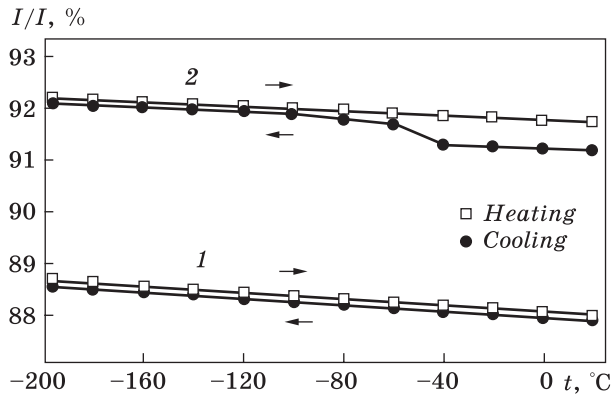

Fig. 4. The change of the magnetisation of technical iron during cooling and subsequent heating of the initial sample (*1*) and the same sample after LT with surface melting (*2*), where I_0 is the magnetisation of the etalon sample of Armco iron [16]

steels, a reorientation of martensite crystals was previously observed mainly along the direction of the easy magnetisation axis, which contributes to an increase in magnetisation and an increase in the exploitation stability of the tool [56]. However, if the reorientation of crystals in a certain predominant direction during magnetic-pulse treatment occurred under the action of an external magnetic field, then, during laser melting, it apparently occurred under the action of a temperature gradient.

During LT, local thermal stresses are induced in the surface layers of the material, which change the nature of the domain structure in the regions adjacent to the zones of laser influence [57]. If we consider individual structural components as domains, then the improvement of the magnetic properties of highly-textured iron with a coarse-grained structure is ensured by their crushing, which is characteristic of LT. The fragmentation of domains is carried out mainly due to the impact of a laser pulse, as a result of which regions with an increased density of dislocations are created in the metal, forming new domain walls, which, in turn, form the closing domains. The main contribution of the domains is that it plays the role of nuclei in the magnetisation reversal process [58]. Magnetostructural barriers introduced after LT in the direction perpendicular to the texture axis create additional magnetic flux stray fields, serve as a source of re-magnetisation, and significantly reduce the total magnetic losses [57]. The reason for the increase in magnetisation after LT may also be the formation of nitrides and oxides, since their magnetic moment is higher than that of pure iron.

To study the degree of stability of the γ-phase contained in samples of Armco iron after laser melting, with respect to the subsequent γ–α-transformation, x-ray studies of such samples were carried out both after cooling to cryogenic temperatures (–185 °C) and after heating to higher temperatures (200–800 °C) [59, 60].

Low-temperature x-ray investigations of cylindrical coarse-grained samples (2–4 grains per sample) with a diameter of 0.6–0.7 mm were carried out in a low-temperature x-ray rotation chamber for single crystals [61]. The chamber is designed for x-ray study of phase and structural transformations occurring with the fulfilment of crystallographic orientation relationships between the crystal lattices of the transforming phases. The design of the chamber made it possible to rotate the cooled sample during x-ray diffraction process, as well as swing it in a given angular range of the chamber limb, photographic recording of the main x-ray reflections from the faces of the crystal lattice and stabilization of temperatures in the range from temperatures close to the temperature of liquid nitrogen (–185 °C) to room temperature with an accuracy of no worse than 0.5 °C. The samples were soldered with Wood's low-melting solder into a holder installed at the bottom of a vessel with liquid nitrogen. A micro-

heater made of nichrome wire with a diameter of 0.1 mm and a power of 20 W was placed on the holder.

Samples with γ-phase after laser melting were kept for six months at room temperature. Rocking x-ray patterns, as well as x-ray patterns from a stationary sample, successively rotated through 2° in intervals of 30°, did not contain signs of γ-phase decomposition. The volume fraction of the γ-phase did not change, and the degree of textural discrepancy between different x-ray reflections remained too. The magnetisation of such samples did not change for six months. These facts indicated that γ-iron obtained by laser self-hardening is quite stable at room temperature.

After cooling in liquid nitrogen, the γ-phase was no longer fixed by x-ray photography at room temperature, because the temperature at the end of the martensitic γ–α-transformation was below room temperature. At the same time, it was not possible to observe x-ray reflections from the α-phase formed from the γ-phase upon cooling in the form of isolated reflections (as from single-crystal regions) because they were superimposed on the continuous Debye lines from the polycrystalline α-phase component formed by laser autohardening. For this reason, it was not possible to determine the orientation relationships between the crystal lattices of γ- and α-phases. However, there is a reason to assume that they are close to the Kurdjumov–Sachs relations, as was the case in steels containing carbon in an amount close to the amount of nitrogen in the studied samples [51].

Subsequently, x-ray studies of samples with the γ-phase were carried out with a successive decrease in temperature below room temperature. A decrease in the intensity of the reflexes of the γ-phase was observed with a decrease in temperature to approximately –10 to –30 °C. At the temperatures from –40 to –50 °C, the reflexes of the f.c.c. γ-phase were no longer recorded.

The magnetisation of Armco iron increased with decreasing temperature, and, when warmed from −196 °C, it was restored (Fig. 4, curve *1*). The magnetisation of the samples, in which the γ–α-transformation took place upon cooling, increased irreversibly in the approximately same temperature range, in which the weakening and disappearance of the γ-phase reflexes were observed (Fig. 4, curve *2*). This meant that the increase in magnetisation upon cooling is associated with the formation of a magnetic α-phase from the γ-phase. Subsequent heating of the samples from liquid nitrogen temperature to room temperature led to a decrease in magnetisation (heating curve). Repeated cycles fulfilment of samples cooling to −196 °C and heating to 20 °C were accompanied by a change in magnetisation along the same curve characterising its temperature dependence.

X-ray study of samples at room temperature after successive heating to higher temperatures and cooling in cold water indicated that the γ–α transformation in such samples also occurred during heating. Heating to 200–400 °C did not change the intensity and angular position of the α- and

γ-phase reflexes. After holding at 550 °C for 10 min, no reflexes of the γ-phase were observed. The change in the magnetisation of a sample heated to 500 °C and cooled in cold water showed an increase by 3–3.5%. From this, it followed that after laser melting, the γ–α transformation was realised in the process of cooling of the sample to room temperature.

5. Formation of Microstructure of the Steels as a Result of LT

The structural state of the surface layer treated by the laser determines the whole complex of physical, mechanical and operational characteristics of the surface of the detail. The main regularities of the structure formation of steels after LT by both continuous and pulsed radiation are described in the literature. Herewith, LT with milli- and nanosecond pulses leads to subtle phase and structural changes, to a more developed substructure, which is due to rather high heating–cooling rates and a significant nonuniformity of the temperature gradient along the depth of the laser influence zone (LIZ). Taking these features into account, one can expect the formation of a structure qualitatively different from the previously studied structure under pulsed LT.

In the works [49, 51–53, 60], the microstructure of steels and their mechanical properties were mainly analysed in the end plane along the depth of the LIZ. This methodological approach is determined by the practical interest in the issues of wear of the surfaces of details after LT. In some cases, it is important to study the regularities of microstructure formation on the working surface of a detail, *i.e.*, in the LT plane. In this case, it is of practical importance to study the influence of the parameters of pulsed laser heating, in particular, the energy and the multiplicity of pulses, on the character of the microstructure, its uniformity in the hardened layer, and the microgeometry of the surface. The results of such studies can be useful in determining the regularities of the relationship between the LT regimes and the structural and phase state of the irradiated layer, as well as the complex of its physical and mechanical characteristics.

LT by single pulses with surface melting leads to the formation of a laser spot microstructure bounded by an irregularly shaped circle. None of the numerous experiments succeeded in forming a strictly circular laser spot on the sample surface. This was due both to the inhomogeneity of the structure and properties of the surface layer of the sample, and, to a greater extent, to the uneven distribution of energy over the laser beam cross section. It should be noted that when using two active elements of a circular cross section, the unevenness was 10%, and when using a solid active element of a rectangular cross section, it was only 5%. In accordance with this, the deviations of the shape of the laser spot from the geo-

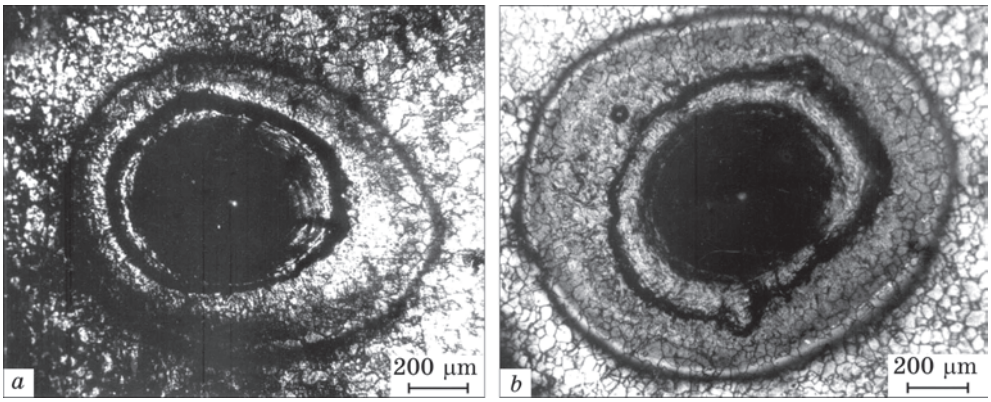

Fig. 5. Microstructure of Armco iron in LIZ after LT with energy density of 3 (*a*) and 6 (*b*) J/mm^2 [60]

metric circle were somewhat smaller when active elements of a rectangular cross section were used. During treatment by a series of several pulses and repeating the melting–crystallisation cycles, the noncircularity of the laser spot increased due to the change of the energy distribution in successive pulses.

Two zones were clearly observed in the structure of the laser spot after LT with an energy density of 3–23.6 J/mm^2: the transition zone and the remelting zone (Fig. 5). The boundaries of the zones were quite clear and were well etched even with a short exposure time in the etchant. This indicated the accumulation of a significant number of defects along the boundaries of the zones.

The initial sample of Armco iron contained equiaxed grains of 50–100 μm. The size of the grain at the boundary of the transition zone was retained in comparison with the initial, before LT, state, and its microstructure differed from the initial one only by greater etchability. Separate grains were observed, through which the boundary of LIZ and the initial metal passed. Such grains did not have discontinuous or broken boundaries.

In the transition zone, a noticeable refinement of the initial structure took place, but the structural transition was not smooth, as might be expected, but stepped, with a jump in grain size up to 3–5 μm. The crushed grains of the transition zone in most cases are formed inside the boundaries of the original grains; this indicates the absence of significant diffusion mixing [62–68]. The intermittent change of the structure, apparently, was associated with significant cooling rates, when the thermal stress fields propagating in the form of concentric circles from the centre of the laser spot changed their magnitude stepwise.

The remelting zone was separated from the transition zone by a fairly wide boundary. The remelting zone at energy densities up to 5 J/mm^2 was

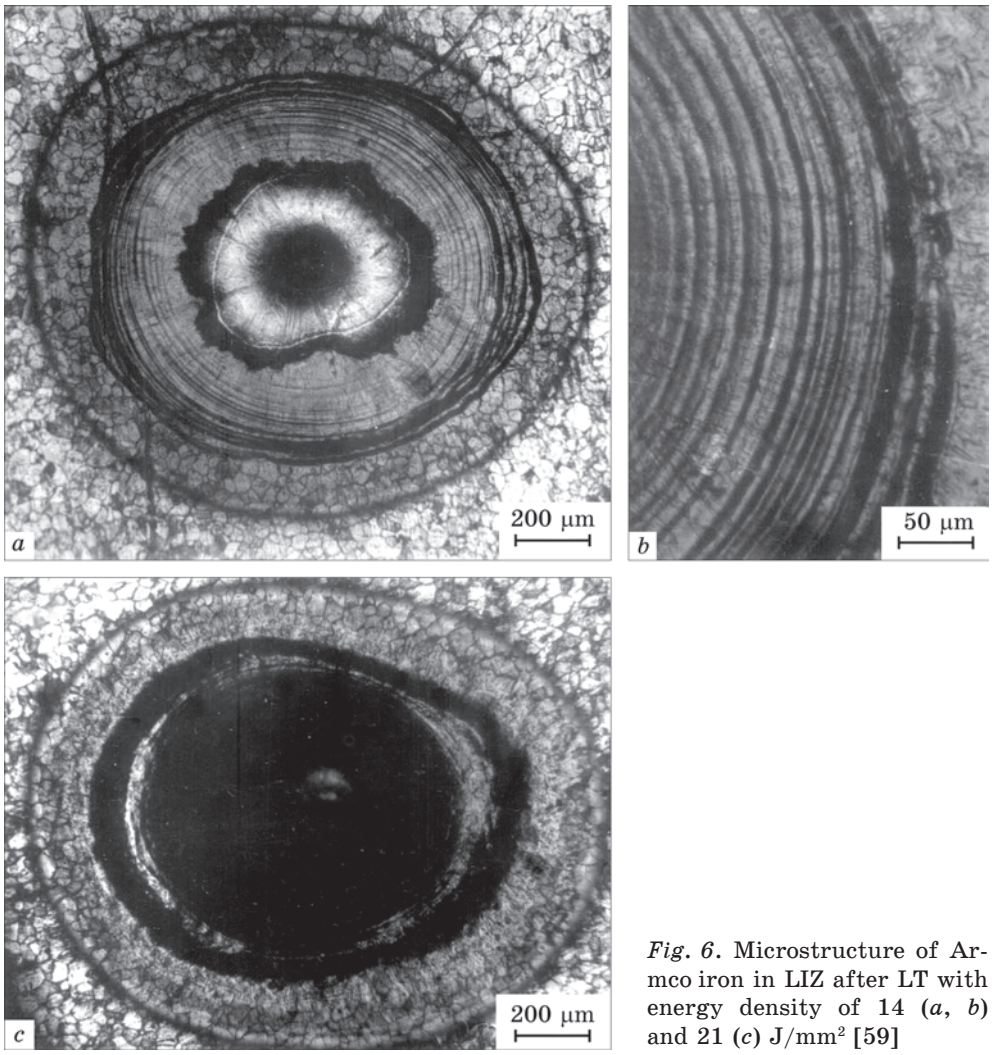

Fig. 6. Microstructure of Armco iron in LIZ after LT with energy density of 14 (*a*, *b*) and 21 (*c*) J/mm^2 [59]

a convex cone-like weakly etched formation formed as a result of crystallisation of the molten metal. The microhardness of this zone was of 3.1–3.2 GPa (with an initial value of 1.5–1.6 GPa), and its dependence on the spot diameter was a curve with a maximum at the centre. The microhardness of the transition zone in Armco iron increased insignificantly and was of 2.0–2.2 GPa.

With a subsequent increase in the energy density of laser radiation, the diameter of the laser spot and the width of the transition zone increased. Significant changes in the diameter of the melt zone were not observed (Fig. 5, *a* and *b*). Apparently, this is due to the peculiarities of the distribution of laser energy in the beam.

In the range of energy densities of 6.3–19 J/mm^2 in the structure of the laser spot, in addition to the described zones, a zone was observed consisting of waves that arose on the surface of the melt (Fig. 6, *a*), which can be conditionally called surface waves. The central part of the melt zone had a crater form, indicating the ejection and evaporation of metal from this area. This is characteristic of thermal laser impact. The ejected metal formed a shaft of about 50–100 μm high, similar in etchability to the 'white layers' structure. Surface waves were concentric closed circles of irregular shape; the height of their crests was of 5–10 μm. The distance between them increased monotonically with distance from the centre of the laser spot. In various experiments, the number of waves ranged from 3 to 25 (Fig. 6, *b*). The measurement of microhardness on the surface of wave crests was associated with significant methodological difficulties due to the small surface of their peaks, which did not allow the formation of a normal indenter imprint. Such an imprint appeared only when the top of the crests was ground down to a depth commensurate with the height of the crests. Microhardness measurements on the surface of the ground crests showed no difference compared to neighbouring areas of the laser spot.

Consequently, the appearance of the described waves is not associated with liquation of the chemical composition or other inhomogeneities of the melt, but is determined only by the features of the propagation of shock waves in the liquid bath of the melt. Etching or grinding off the laser spot area to a depth of 100 μm did not reveal any traces of surface waves in the metal bulk. This testified to the surface nature of the wave structure.

It was shown in Ref. [69] that, in a layer of molten metal upon heating by concentrated sources, in addition to ordinary gravitational–capillary waves, the natural frequency of which is determined by the dependence [70]

$$\omega_0 = \sqrt{Ik + \frac{\sigma k^3}{\rho}}, \qquad (4)$$

there are also thermocapillary waves, *i.e.*, weakly damped surface waves with a dispersion law of sound type:

$$\omega \propto k\sqrt{\frac{dT}{dz}}, \qquad (5)$$

where I is a power density, k is a wave vector, σ is a coefficient of surface tension of the melt, ρ is a density, T is a temperature, and z is a crystallisation co-ordinate.

From the resonance condition, the maximum frequency of the resulting surface waves is $\omega_M = \omega_0 k/2$. For iron and steel at $I \cong 10^5$ W/sm^2 and $k \cong 10^2$ cm^{-1}, ω_M will be equal to $\cong 10^3$ Hz [71]. Therefore, the frequency of these oscillations is quite high, and they can be observed, when the sample is melted by pulsed laser radiation of the millisecond range ($1/\omega_M = 10^{-3}$ s), which corresponds to the irradiation conditions in our case ($t_{imp} = 8 \cdot 10^{-3}$ s).

A similar wavy structure was observed in the case of through piercing of thin aluminium foils [72], with surface LT of niobium [73] and DIN 105 WCr 6 [74]. In Ref. [72], a wavy structure was formed on both sides of a foil of thickness h satisfying the condition $h \ll (c\tau)^2$, where χ is the thermal conductivity and τ is the laser pulse duration. With an increase in the foil thickness in similar irradiation regimes, this structure was not observed. All works, in which a surface wavy structure was observed, are united by the fact that the treatment was carried out by pulsed radiation with pulse duration of the same order (~10^{-3} s). In the case of laser treatment in the free generation mode (in the presence of spikes in the pulse), wave fixation was not observed [73].

There is no consensus on the influence of the energy characteristics of laser radiation on the conditions of the formation of a wavy structure. In Ref. [73], it was concluded that the higher the radiation flux density, the more pronounced the wavy structure. But, on the other hand, it was found that there is a certain limit or critical energy density [69], above which the wavy structure was not fixed, because destruction of the metal surface with abundant vaporisation began. Based on an analysis of resonance conditions for waves of two types in Ref. [69], the threshold value of the power density was calculated (for iron and steels, W_p = 3 kW/sm^2), at which conditions are created for the formation of an unstable wavy structure on the surface. Therefore, we can tell about the existence of two threshold values of the energy density, lower and upper, in the range of which conditions are created for the formation of a surface wavy structure. For our experiments, these values are equal to 6.3 J/mm^2 — the lower limit of the energy density, up to which the wave structure was not observed, and 19 J/mm^2 — the upper limit, above which a crater was formed (Fig. 7). Note some stability of the number of waves of 7–10 in the range of energy densities 11–18.9 J/mm^2.

Estimated recalculation of energy density into power density W_p (in W/cm^2) can be performed according to the dependence [75]

$$W_p = \frac{4E}{\pi d^2 \tau}, \tag{6}$$

where E is energy of laser radiation per pulse (J); τ is pulse duration (s); d is diameter of the laser spot (cm). For energy values of 4 and 12 J (at $\tau = 8{-}10^{-3}$ s and d = 0.09 cm), the estimated values of the lower and upper thresholds of power density will be equal to 78.6 kW/sm^2 and 235.7 kW/cm^2, respectively, that agrees satisfactorily with the calculation data in Ref. [69].

The appearance of a wavy structure is associated with the instability of the melt surface that occurs in a vapour flow during thermal shock [72], which is associated with the development of vortex gas-dynamic perturbations. In this case, apparently, the effect of self-oscillations [76] has a certain significance, which consists in the fact that, when the metal is

heated by laser radiation with an energy density exceeding a certain critical value, the temperature on the melt surface begins to fluctuate. The presence of temperature fluctuations, which are weakly damped in time, indicates the existence of resonant metal heating modes and has the following interpretation. Under laser treatment, the maximum temperature is at the depth of metal in the near-surface layers. If the perturbation of the surface is a depression, then, the temperature in this place increases, because this section corresponds to a more heated zone. With an increase in temperature, the evaporation rate increases, the depression increases, and this area heats up even more, which contributes to the next cycle of evaporation–heating [71].

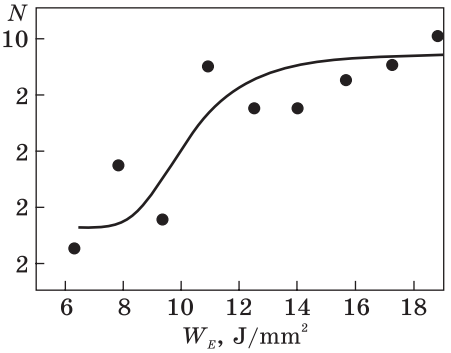

Fig. 7. The number of surface waves *vs.* the energy density [60]

From our point of view, it is technologically expedient to use a developed wavy structure to retain lubricant at the points of contact of rubbing surfaces.

An increase in laser energy density in the range of 14.9–19 J/mm^2 led to the fact that the crater formed in the central part of the laser spot began to grow, indicating an increase in the volume of evaporated metal. At this, the formation of additional surface waves was observed mainly on the periphery of the remelting zone. The structure in this range of energy densities is interesting in that a large number of columnar dendritic crystals were observed at the place of crater formation (Fig. 8). The orientation of axes of these crystals was both regular, towards the heat removal, and chaotic. This indicated a significant inhomogeneity of the temperature gradient in the plane of the laser spot. Radial orientation of the axes

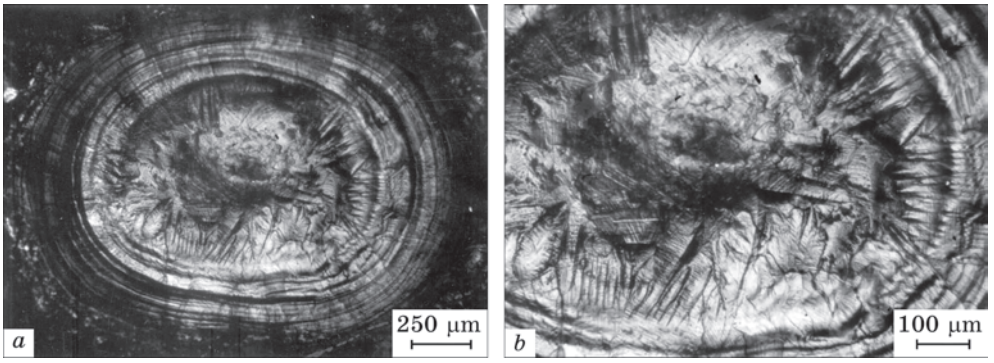

Fig. 8. Microstructure of Armco iron in LIZ after LT with an energy density of 17 J/mm^2 [16]

of columnar crystals from the centre of the laser spot to the initial matrix was observed in the transition zone.

The features of crystallisation during pulsed LT are that a large temperature gradient and supercooling appear at the melt–initial matrix interface, which promote the growth of columnar dendritic crystals in the direction of heat removal, *i.e.*, perpendicular to the edge. In the direction of heat removal, crystals begin to grow first and grow faster than in other directions. In the centre of the laser dimple, there is no definite sharp direction of heat removal; the metal is retained longer in the form of a melt, which contributes to its local mixing under the action of thermocapillary forces [69].

It is known from the theory of crystallisation that only some of the initially formed crystals are nucleated on the mould wall [77]. If the wall of the mould is inferior in its ability to form nuclei to particles in the melt, then, crystallisation centres are formed only in the bulk of the liquid and begin to grow towards the walls.

During local laser heating, the formation of a melt in a massive matrix contributes to the fact that the crystallisation front begins at the boundary of the maximum heat removal from the melt–initial matrix and moves towards the centre of the laser hole. In this case, one of the first to form is columnar crystals growing in the direction of the heat removal. In addition, the process of crystallisation in the laser hole is affected by the mixing of the liquid, as evidenced by the formation of a finely dispersed structure and surface waves. During the short time of the laser pulse action, the metal quickly heats up to the melting and boiling point.

Similar regularities of crystallisation were observed in the melt during its rotation in the mould by means of electromagnetic stirring [77]. The rotation of the liquid phase during its crystallisation was accompanied by a decrease in the grain size and a reduction in the length of the columnar zone; the columnar zone inclined toward the interface in the direction of rotation. If the crystallisation of the melt began after the rotation of the liquid at a constant speed was established, the usual coarse-grained structure was formed, which is characteristic of a fixed-mould casting. However, a periodic change in the direction of rotation led to the formation of a finely dispersed structure due to viscous shear in the liquid.

Apparently, an equiaxed finely dispersed structure can be obtained at any stage of crystallisation by forced shear of the liquid relative to the solid phase. On the one hand, this can be explained by the breaking off of the tips of dendritic crystals under the action of the generated viscous forces; on the other hand, apparently, the convection effect of mixing on crystals already growing in the liquid and faster cooling of the liquid due to the intensification of heat removal to the columnar zone. Increasing the energy density above 20 J/mm^2 again led to the formation of two zones, the central of which (remelting zone) was a crater of considerable size

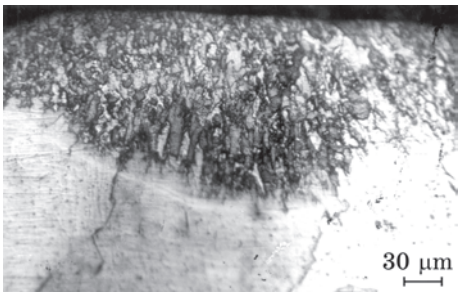

Fig. 9. Microstructure of Armco iron in LIZ after LT with an energy density of 14 J/mm^2 [52]

(Fig. 6, *c*). At this point, the thermal zones and boundaries between them were preserved.

To reveal the fine-grained structure in the LT plane, the surface relief of the laser spot was ground down to a depth of 20–50 μm, counting from the maximum peaks, and subjected to chemical etching. End sections were prepared by forming a chain of laser spots in the immediate vicinity of the end edge and grinding the indicated edge almost to the centre of the laser spots, followed by polishing.

Metallographic observations showed that a high cooling rate after laser melting led to the formation of a more finely dispersed structure with certain regularity in the grain size distribution over the LIZ. Previously, it was shown that LT in the continuous mode is characterised by strong block refinement and a certain size distribution of structural components. In this case, two distinct layers were observed, which differed in the degree of completion of phase transformations. In the case of pulsed treatment in the LIZ, as in the LT plane and in the end plane, three layers with different grain sizes were observed. It should be noted that, in the end plane, the LIZ had a phial-like shape with a modified structure, the total depth of which for the indicated treatment modes did not exceed 160–180 μm. When considering the change in the structure along the depth of the LIZ, it is easy to see the three indicated layers (Fig. 9). The first layer up to 15–20 μm deep was characterised by finely dispersed equiaxed grains with an average size of 1.5–3 μm (Fig. 10, *b*). The second layer up to 100 μm deep had larger grains with an average size of about 10 μm. The third layer located at the boundary of the LIZ is the initial matrix consisted of grains elongated along the heat removal axis with a diagonal of about 20 μm.

The physical essence of the formation of mainly three layers with different grain sizes in the laser-melted zone appears as follows. During laser melting, due to high cooling (crystallisation) rates, there was a predominant growth of the main axes of dendrites directed perpendicular to the melt–initial matrix interface, which formed the third layer of columnar crystals. At the same time, in the upper near-surface layers of the laser dimple, due to the lower temperature gradient and oscillatory motions of the melt, the metal was in a liquid state for a longer time and was mixed. These processes led to significant grain refinement due to phase $\alpha \leftrightarrow \gamma$ recrystallization and, possibly, plastic deformation under the action of thermal stresses followed by recrystallization. All this contributed to the

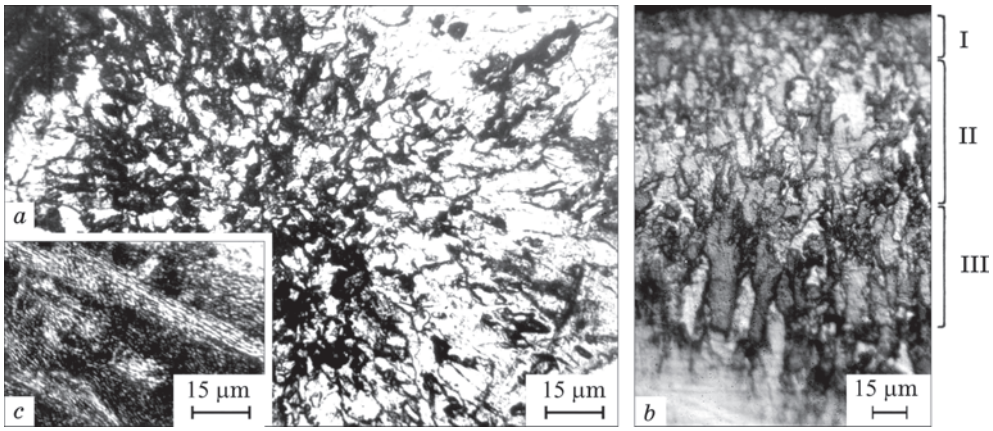

Fig. 10. Microstructure of Armco iron in LIZ after LT with an energy density of 14 J/mm^2, where *a* and *c* — in the plane of treatment at a depth of 20–50 μm, *b* — in the plane, which is perpendicular to the plane of treatment. Here, fragment *b* is from Fig. 5; I, II, III denote layers with different size dimensions [52]

formation of the first near-surface layer with a finely dispersed equiaxed grain.

In the LT plane, a certain distribution of structural cells was observed in the radial direction (Fig. 10, *a*). Although the grain boundaries in this case were etched more strongly, especially, in the central part of the laser spot, some grains, mainly in the zone of columnar crystals, did not etch easily, even with etched boundaries.

The initial microstructure of Armco iron consisted of large grains of ferrite and cementite, which were located at the boundaries of ferrite grains in the form of an edge. After LT, the microstructure of the spot in the melting zone was crushed ferrite, along the newly formed boundaries of which, near cementite areas, dark-etched martensite packets were formed, indicating the formation of austenite in these areas during heating (Fig. 10, *c*). During pulsed laser heating, the appearance of austenite regions with increased carbon content probably occurred only near individual cementite particles. A similar regularity in the structure formation of martensite in Armco iron was observed in Ref. [78] after treatment with a continuous CO_2 laser. The formation of a martensitic structure was observed mainly in the near-surface layers in the LT plane. Thus, the microstructure of Armco iron after pulsed LT can be highly inhomogeneous due to the short time required for diffusion alignment of the composition of resulting austenite and is determined by the local distribution of cementite along the boundaries of ferrite grains in the newly formed structure.

Some features of the structure formation of Armco iron during LT by a series of several pulses were identified. The number of pulses in different experiments varied from 3 to 10 with a frequency of 0.5–1 Hz. Quali-

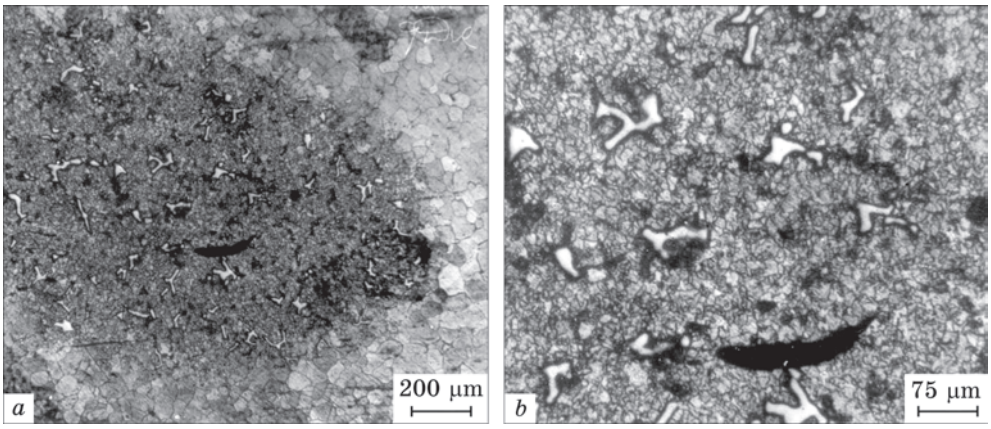

Fig. 11. Microstructure of Armco iron in the plane of LT by series of pulses: number of pulses — 3, energy of pulse — 9 J [19]

tative changes in the character of the structure were discernible after the fourth pulse. In this case, an equiaxed finely dispersed structure with a grain size of <5 μm was formed (Fig. 11, *a*) as well as, additionally, a structure similar to the eutectic (Fig. 11, *b*). The eutectic was observed only in the LT plane in the near-surface layers. The contours of eutectic formations were also seen on the microstructures after LT by a single pulse in the transition zone. As a result of treatment by a series of laser pulses, the eutectic was more formed and represented distinct formations with a size of ≈50 μm. The eutectic grew predominantly along the boundaries of the initial ferrite grains, exactly where the initial structure contained carbon. It is known that, regardless of the initial carbon composition of the steel, the first portions of the formed austenite always have a composition corresponding to the state diagram and close to eutectoid (0.7–0.8% C) [27]. It can be assumed that the melt was also saturated with interstitial atoms from the atmosphere. The microhardness of the newly formed finely dispersed structure was of 2.6–2.7 GPa, but the microhardness of the eutectic formations was somewhat higher and amounted to 3.1–3.3 GPa.

Thus, in the case of a pulsed LT with a series of several pulses, the exposure time is quite sufficient for the diffusion redistribution of carbon in the near-surface layers and the creation of regions with a carbon concentration close to the eutectic one.

In the case of LT by a series of pulses, the process of formation of a laser dimple in depth was also of interest. In a metallographic study on the end plane after pulsed LT, a correlation was noted between the number of crystallisation zones and the number of laser pulses (Fig. 12). In some cases, the number of crystallisation zones separated by fairly clear boundaries corresponds to the number of pulses. If, for example, the treatment

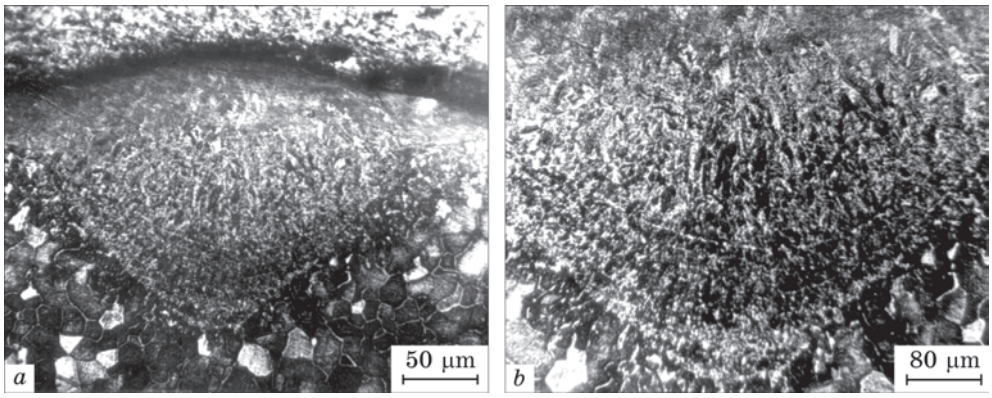

Fig. 12. Microstructure of Armco iron in LIZ after multiple LT. Number of pulses — 5, energy of pulse — 9 J [19]

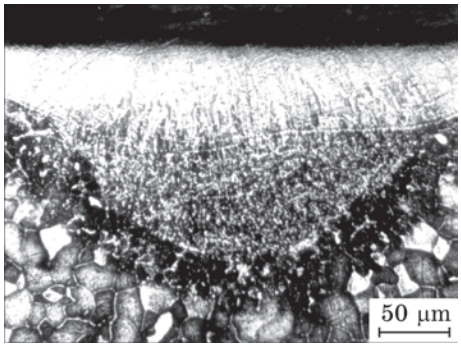

Fig. 13. Microstructure of Armco iron in LIZ after multiple LT. Number of pulses — 5, energy of pulse — 10 J [81]

was performed by a sequence of five pulses, then, five crystallisation zones could be distinguished on the structure by the depth of LIZ. Under some modes of multiple LT, the first zone contained white layers of structureless high-carbon martensite with increased microhardness (Fig. 13).

The initial microstructure of AISI 1035 steel was a mixture of ferrite and pearlite. Obviously, during high-speed laser heating, austenite was the first to form in pearlite regions. Due to the uneven temperature gradient along the depth of the laser hole, the upper layers were at a high temperature for a longer time. It was in these zones that pearlite first turned into high-carbon austenite, and when cooled, into structureless martensite with high microhardness (Fig. 14). The microhardness of light areas of structureless high-carbon martensite was 2 times higher than the initial one and amounted to 2.9–3.2 GPa. According to the literature data, structureless martensite obtained after LT consists of lenticular crystals of 0.2–1.0 μm wide [78]. The near-surface layers of structureless martensite, when advancing along the depth of the LIZ, passed into a zone with the structure of low-carbon martensite, which was formed mainly from ferrite. The highest carbon structure based on the microhardness curves (Fig. 14) was at a depth of 20–40 μm. Therefore, at high-speed LT, there are additional factors that allow, in such a short time, the mass transfer of carbon.

It is known that, in the case of LT with several pulses, the carbon content in the solid solution increases and becomes comparable with its

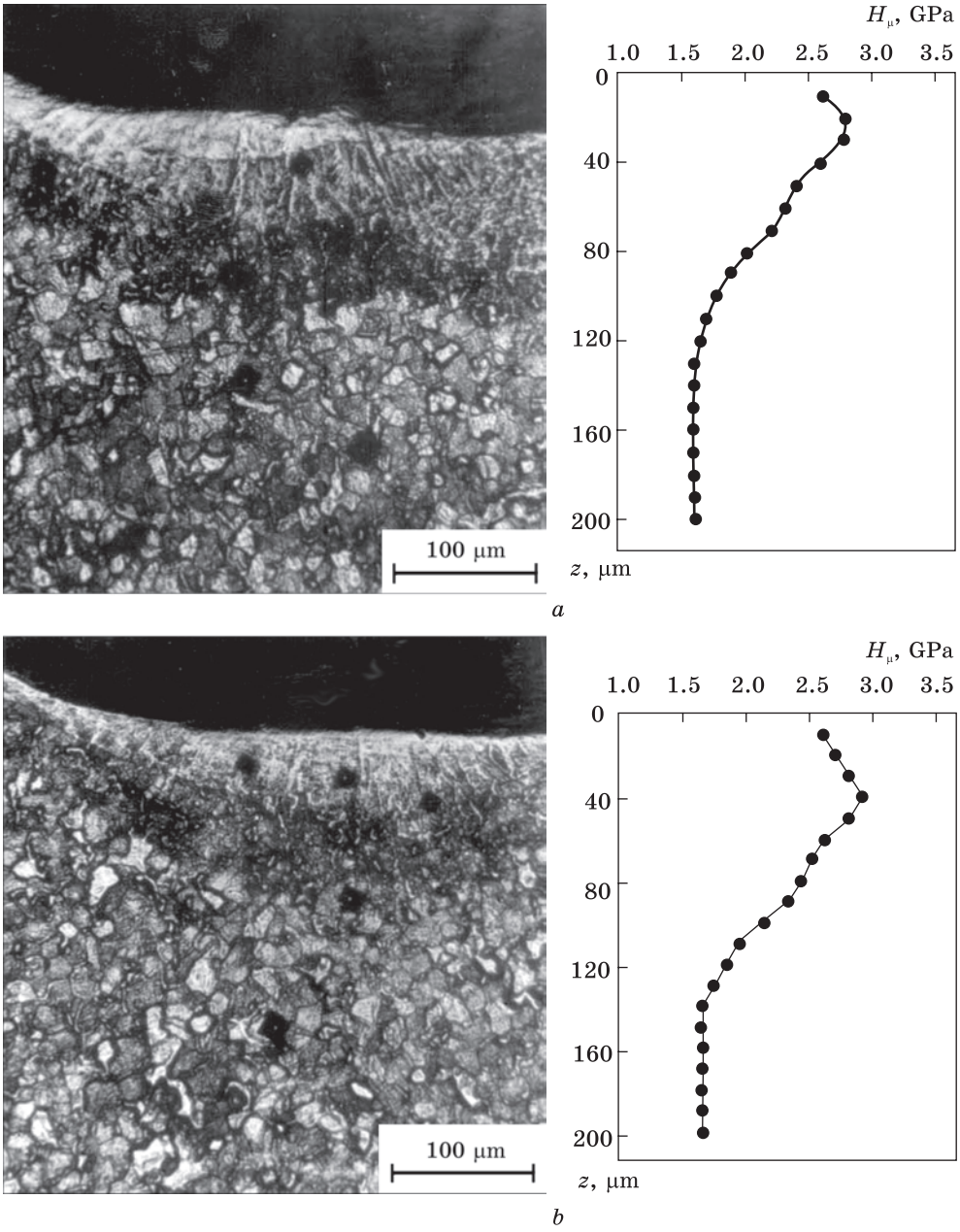

Fig. 14. Microstructure of AISI 1035 steel in LIZ and microhardness over the depth after LT with energy density of 11 (*a*) and 14 (*b*) J/mm^2 [16]

average content in steel [79]. When treatment of AISI 1035 steel with a series of several pulses done, a gradual delamination of the newly formed structure occurred with the formation of clear boundaries (Fig. 15). In

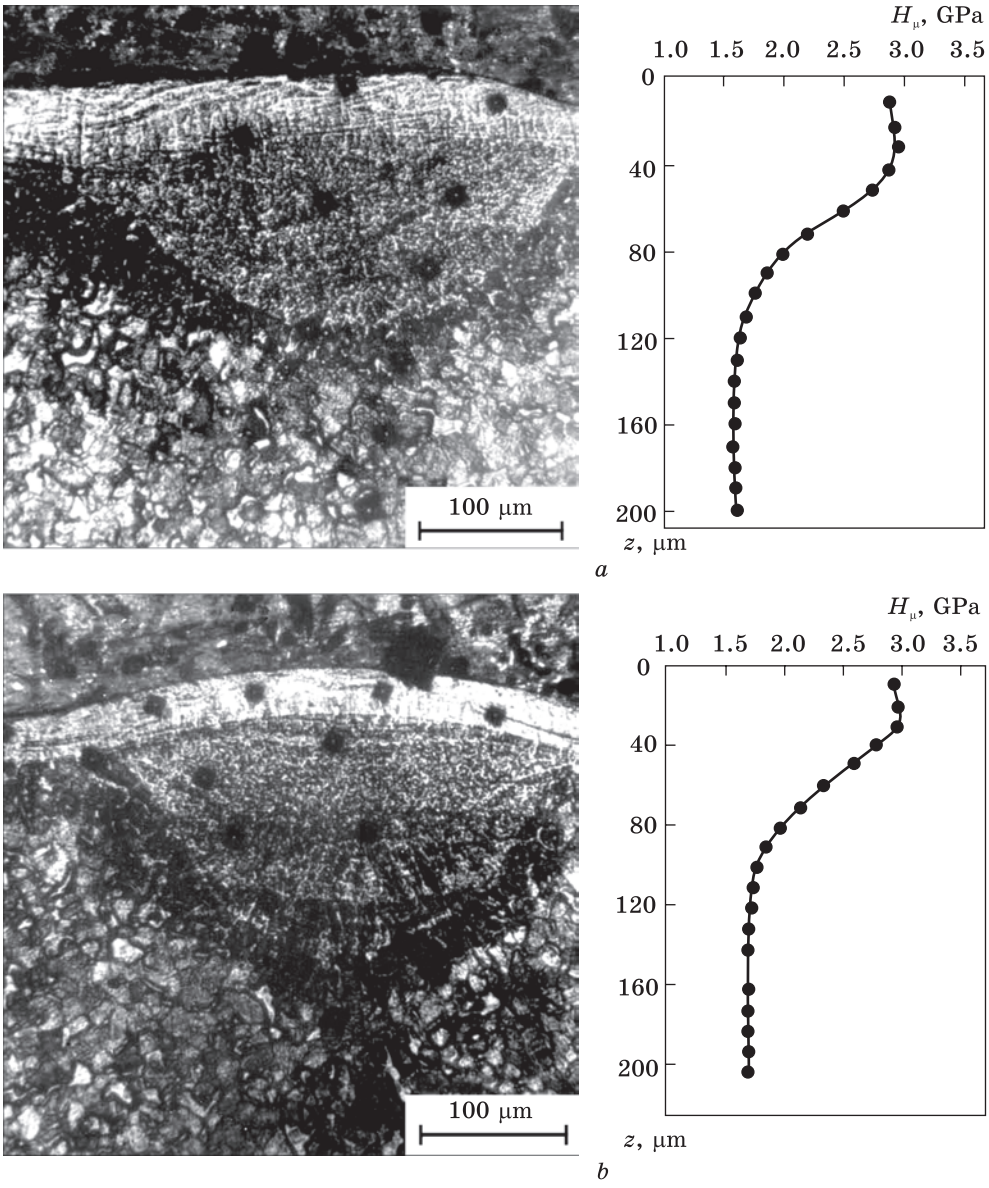

Fig. 15. Microstructure of AISI 1035 in LIZ and microhardness at depth after multiple LT with the number of pulses 5 (*a*) and 10 (*b*) for the pulse energy of 9 J [16]

this case, the following were clearly distinguished: a near-surface, ≈30 μm thick, white layer of high-carbon structureless martensite with high microhardness, several zones of low-carbon dark-etched martensite with different carbon content, and a fine-dispersed ferrite–pearlite mixture, which passed into the initial structure. The correlation between the number of

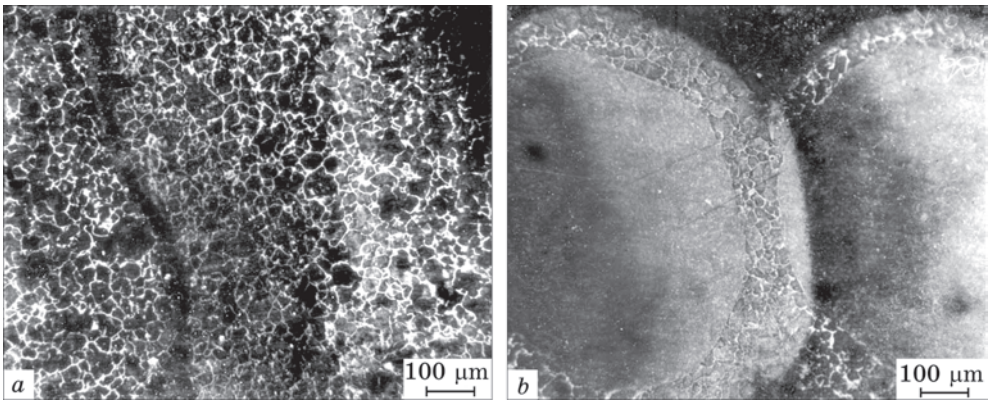

Fig. 16. Microstructure of AISI W110 steel in LIZ after LT without melting (*a*) and with melting (*b*) of the surface. Energy density is of 2.4 and 9 J/mm^2, respectively [51]

crystallisation zones and the number of laser pulses, established for Armco iron, was preserved for AISI 1035 steel.

Features of structure formation in hypereutectoid AISI W110 steel with an initial pearlite–cementite structure during LT were observed along the laser path. After LT without melting, no changes in the grain structure in the treatment plane were observed. However, in the metal heated to the austenitic state, carbon was redistributed along the direction of the laser beam. In the microstructure, the longitudinal redistribution of carbon along the laser path was observed as an alternation of light and dark areas. Probably, high-carbon austenite formed at the site of the initial cementite light zones (Fig. 16, *a*), and less carbon-saturated austenite and cementite formed dark zones.

The effect of carbon redistribution along the laser track was intensified in LT with surface melting. The contours of the carbon-enriched and depleted zones were more distinct (Fig. 16, *b*). In the melting zone, the structure of high-carbon massive martensite was formed in the direction of the laser beam and low-carbon dark-etched areas were formed too. Partial melting of the metal occurred along the boundaries of the laser spots, followed by solidification, probably, into ledeburite eutectic.

Consequently, the local mass transfer of carbon during LT, discovered in Ref. [78], is possible not only along the depth of the LIZ, but also in the direction of radiation moving.

Metallographic studies of AISI W110 steel in the end plane showed that treatment with single laser pulses led to the formation of a white layer only in a narrow near-surface region of about 20–30 μm thick. During LT with a series of pulses, the thickness of the white layer increased significantly. This layer had a massive martensite structure with a high microhardness of 8–10 GPa (Fig. 17). The white layers were located starting from the surface of the laser dimple, confirming the assumption that,

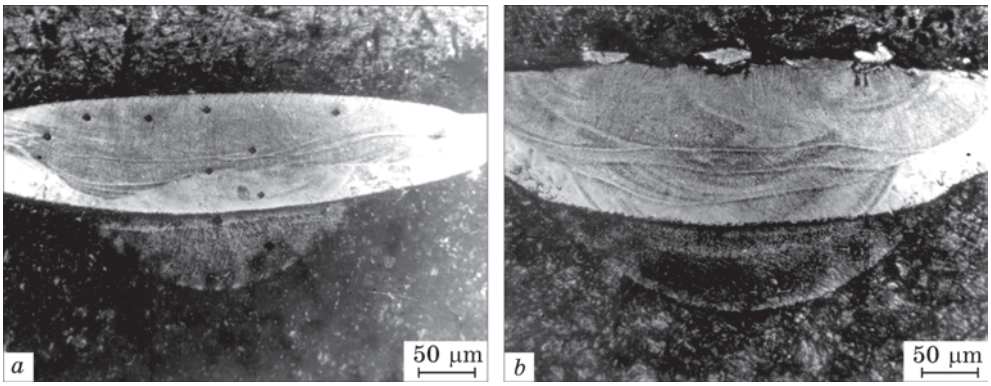

Fig. 17. Microstructure of AISI W110 steel in LIZ after multiple LT. The number of pulses — 5 (*a*) and 10 (*b*); pulse energy — 9 J [51]

during high-speed laser heating, it is in the near-surface layers and conditions are created for saturation of austenite with carbon due to a longer holding time. In addition, a characteristic feature of LT steels, regardless of their initial state, is the formation of a large number of high-angle grain boundaries, which appear as a white layer [78]. LT with a series of several pulses contributes to an increase in the number of high-angle boundaries and, as a result, a greater mobility of carbon atoms.

In the structure of the white layers of AISI W110 steel, the boundaries of the crystallisation zones were clearly visible, indicating a gradual, over a series of pulses, homogenization of the solid solution. Apparently, there was no complete equalisation of the carbon concentration. Probably, ultrafast heating, even at multiple LT of steels with different initial states, does not make it possible to obtain a uniform final structure. For this purpose, it is recommended to carry out a preliminary heat treatment, which would level the initial structure [75].

Samples of Armco iron in the initial state had an equiaxed grain structure, the average grain size of which was of 35–50 μm. The presence of a small number of grains with increased etchability may indicate the presence of a pearlite component, which is formed at low carbon content (0.1–0.15%). The dislocation density in the initial samples did not exceed $1.3 \cdot 10^8$ cm^{-2} (Fig. 18, *a*).

An electron microscopic study of the Armco iron structure after LT was performed both in the near-surface layer of ≈ 5 μm in the treatment plane and in the depth of the LIZ. When the surface was irradiated in the mode without melting (W_E = 2.2–2.9 J/mm^2), the near-surface layer was heated in the γ-region. Recrystallization of the initial structure was not observed in this case; however, the internal microstructure represented weakly expressed cells with an azimuthal misorientation of no more than 0.5° (Fig. 18, *b–d*). Ragged boundaries of weakly misoriented fragments

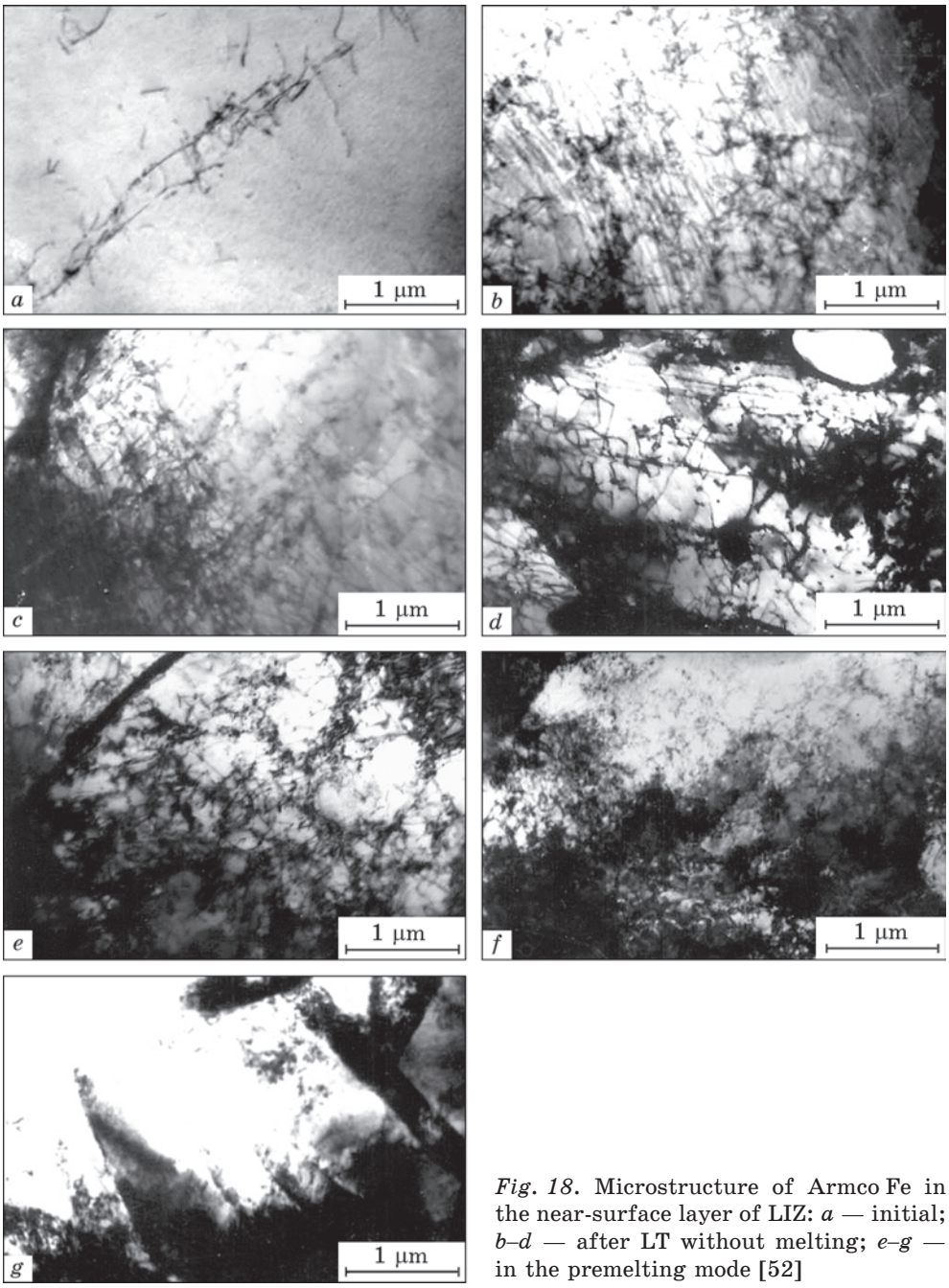

Fig. 18. Microstructure of Armco Fe in the near-surface layer of LIZ: *a* — initial; *b–d* — after LT without melting; *e–g* — in the premelting mode [52]

are formed in some places. After LT without melting, the density of dislocations in the near-surface layer at a depth of about 5 μm increased and amounted to $0.9–1.2\times10^9$ cm^{-2}. The density of dislocations decreased

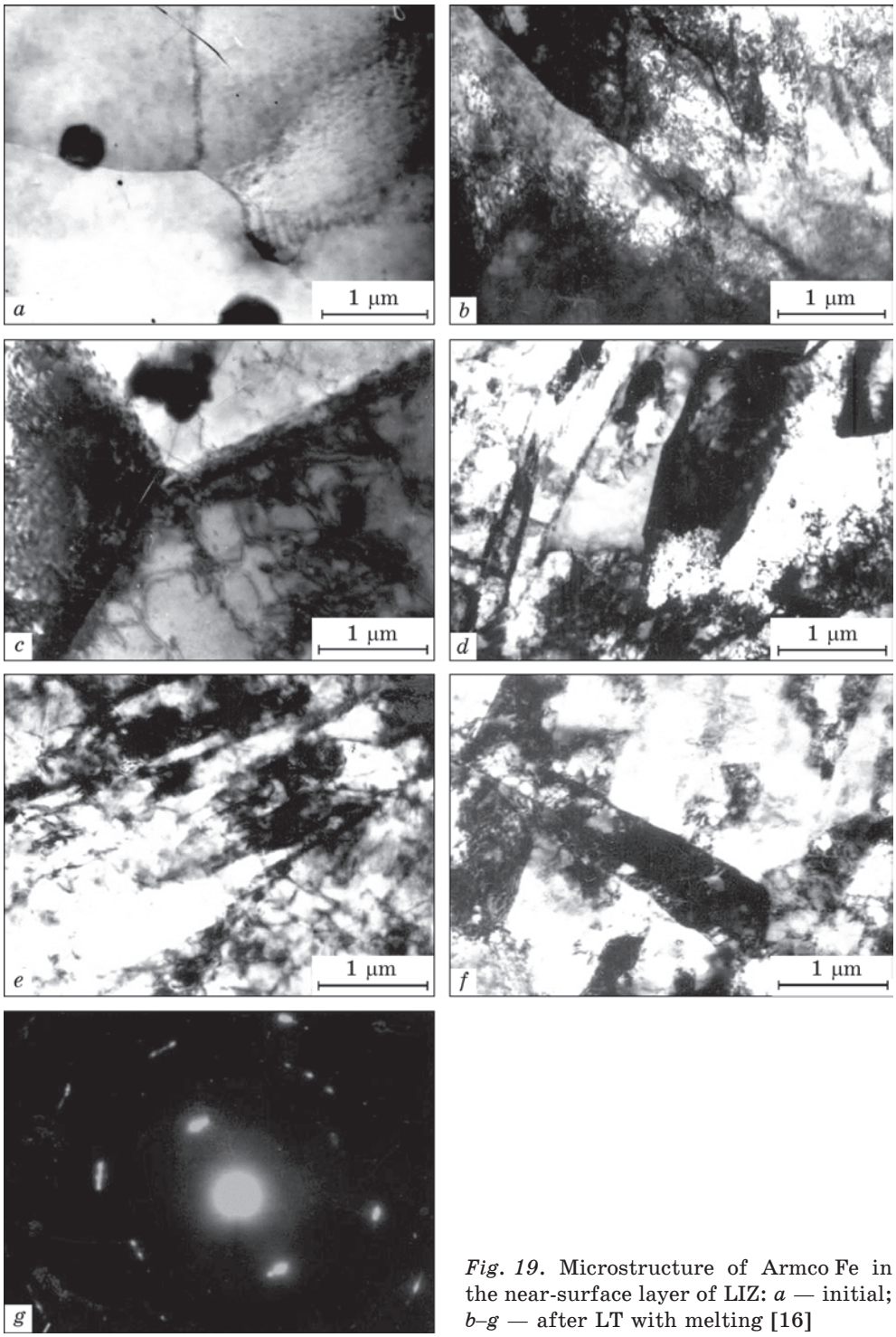

Fig. 19. Microstructure of Armco Fe in the near-surface layer of LIZ: *a* — initial; *b–g* — after LT with melting [16]

somewhat, when moving from the centre of the laser spot to its periphery (Fig. 18, *b*, *d*).

During laser heating of the metal surface in the premelting mode ($W_E \approx 3–5$ J/mm^2), a tendency to the formation of a weakly misoriented cellular structure was observed (Fig. 18, *e*) with a dislocation density increased to 10^{10} cm^{-2} (Fig. 18, *f*). In some cases, quenched structures such as lenticular martensite were fixed predominantly in the centre of the laser spot (Fig. 18, *g*).

During LT with surface melting ($W_E = 12–14$ J/mm^2), recrystallization occurred and accompanied by grain refinement. An increase in the heating temperature in the treatment zone contributed to an increase in the dislocation density up to $0.8–1.2 \times 10^{10}$ cm^{-2} and the appearance of separate sections, morphologically resembling packets of dislocation martensite. The internal structure of grains in this LT regime contained a much larger spectrum of structures, from martensitic to cellular, with an increased density of dislocations. The microstructure of the LIZ in Armco iron after surface melting treatment is shown in Fig. 19. In the central part of the laser spot, the structure of the melt zone was observed (Fig. 19, *f*), which consisted of dispersed (less than 0.5 μm) fragments with an increased density of dislocations. The density of dislocations was high both inside and along the boundaries of the fragments with their significant misorientation. Such a structure can be characterised as dendritic. In some places of the melt zone, the structure of lenticular martensite was observed (Fig. 19, *d*), the formation of which is associated with the presence of local areas with increased carbon content. The martensitic crystals formed during quenching were often twinned that indicated high carbon content within them. In the melting zone, predominantly lenticular twinned martensite was formed, whose crystals were grouped in colonies. In the LT of Armco iron by continuous CO_2 laser, predominantly fine-dispersed packet martensite with a developed block structure was observed [38]. Along the boundary of the melt and transition zones, the structures are shown in Fig. 19, *b*, *e*. The microstructure in Fig. 19, *d* is close to dendritic in nature and may also indicate the presence of both dispersed dendrites and packet martensite. On the periphery of the transition zone, an increased density of defects was observed (Fig. 19, *b*, *c*), which gradually decreased, when moving towards the initial structure (Fig. 19, *a*).

When moving along the depth of the LIZ, the dislocation density increased for both treatment modes, both along the boundaries and inside the cells. At a depth of ≈40 μm, a more pronounced porous structure was observed with centre sizes of 0.5–1 μm and a dislocation density of $1.5–10^{10}$ cm^{-2}. However, deeper than 80 μm, the dislocation density gradually began to decrease, and, at a depth of 120 μm or more, the dislocation structure had a form close to the initial state.

The presented results of an electron microscopic study of the Armco iron structure are in good agreement with the results of microhardness measurements after LT both in the plane of treatment and along the end face of the sample. The increase in microhardness after LT without melting is apparently associated mainly with an increase in the dislocation density. At the same time, a more significant increase in microhardness after treatment with melting, mainly in the central part of the laser spot, is apparently associated with the formation of quenching structures such as lenticular and packet martensite.

6. Mechanical Properties of Steels as a Result of LT

Strengthening of steels during LT is determined by several structural factors, the main of which are an increase in the density of dislocations, dispersion of the structure, the formation of solid solutions with a high content of alloying elements and the formation of excess phases. The structural state of the treated near-surface layer determines the whole complex of physical, mechanical and exploitation characteristics: hardness, wear resistance, corrosion resistance, frictional, strength, plastic characteristics, thermal, magnetic, electrical properties, *etc*.

It is not always possible to determine the mechanical properties of the hardened near-surface layer directly after LT due to significant methodological difficulties. Therefore, in work [53], the yield strength $\sigma_{0.2}$ of the near-surface layer was estimated by calculation based on the experimental characteristics of its structural state.

Armco iron with 0.08% C was chosen as the object of study. An assessment of the hardening factors of the surface layer of such a simple single-phase system as Armco iron is necessary for analysing the mechanism of laser hardening of steels and may be useful in realising the technological resource for increasing the efficiency of LT of construction and tool steels having more complex phase and structural state. In such a system, no precipitation of excess phases was observed and, in addition, there was no solid solution strengthening factor. Consequently, the main strengthening factors in this case were the formation of a fine-dispersed structure and an increase in the dislocation density in α-phase crystals.

Based on x-ray studies, it was found that the period of the crystal lattice of α-iron practically did not change after LT, both in the melting mode and without it, and was of 0.2866 ± 0.0001 nm.

Statistical determination of the grain size d at a certain depth after LT was carried out based on metallographic observations by constructing histograms of the size distribution of structural cells (Fig. 20).

The yield strength of the near-surface layer can be additively represented as the sum:

$$\sigma_{0.2} = \sigma^{\mathrm{I}}_{0.2} + \sigma^{\mathrm{II}}_{0.2}, \qquad (7)$$

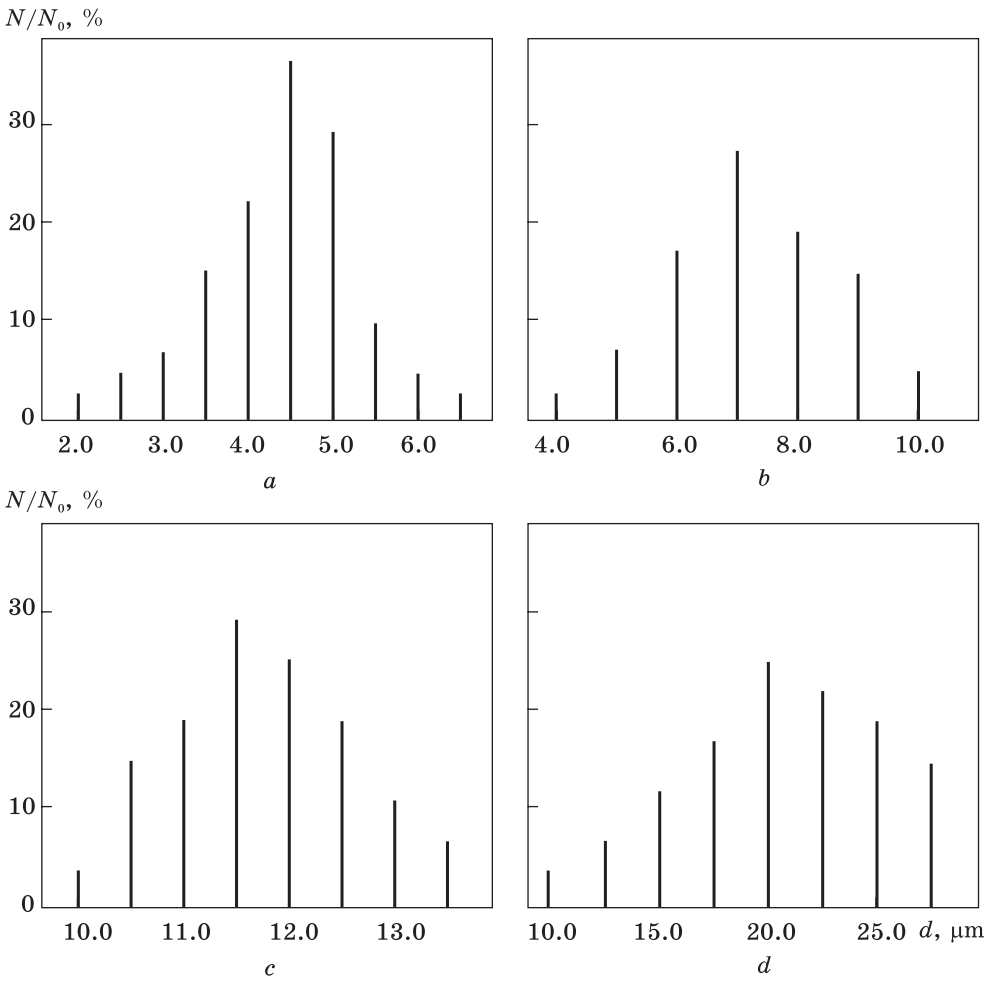

Fig. 20. Histograms of dimensions of the structure cells after LT with surface melting at depths of 20 (*a*), 50 (*b*), 90 (*c*), and 130 (*d*) μm [51]

where $\sigma_{0.2}^{I}$ and $\sigma_{0.2}^{II}$ are the yield strengths dependent on the degree of dispersion and the dislocation density in the structure, respectively.

The first summand in Eq. (7) can be determined from the Hall–Petch equation:

$$\sigma_{0.2}^{I} = \sigma_0 + \frac{K}{\sqrt{d}}, \tag{8}$$

where σ_0 is the yield strength of the initial sample of technical iron, and K is a constant independent of the average grain size d. For calculations, the following values were used: $\sigma_0 = 170$ MPa, $K = 0.19$ MN/m$^{3/2}$.

For calculations, from the histograms, cell sizes were chosen equal to the maximum number of encounters at a certain depth. It turned out that, when the grain size changed from 3 to 25 μm (Fig. 21, curve *1*), the depth

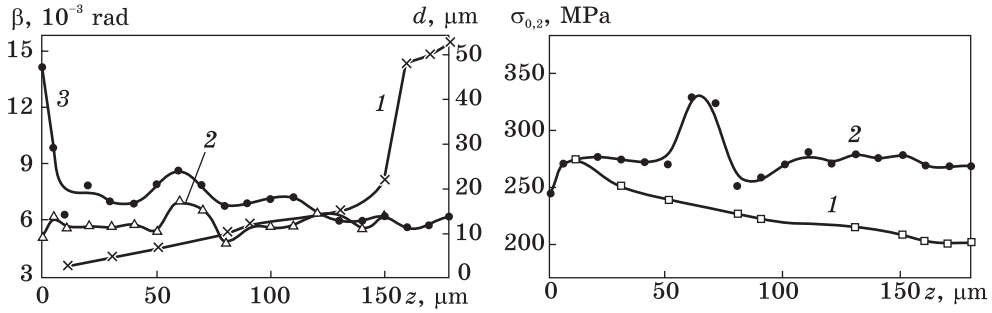

Fig. 21. Change in the grain size d (*1*) and physical broadening β of the $(200)_\alpha$ reflex after LT with melting (*2*) and β after LT without melting (*3*) over the depth of LIZ [24]

Fig. 22 Change in the yield strength $s_{0.2}$ (*1*) and microhardness H_μ measured on the sample end (*2*) and after layer-by-layer etching (*3*) of the Armco iron over the depth of LIZ [90].

of the LIZ $\sigma^{I}_{0.2}$ changed from 280 to 210 MPa, respectively (Fig. 22, curve *1*). These values should be considered as an increase of $\sigma_{0.2}$ for technical iron due to the dispersion of the structure in the process of laser melting. At the same time, $\sigma^{I}_{0.2}$ is increased approximately by 1.2–1.65 times compared to the initial value.

To determine the density of dislocations in the LIZ, the physical widening β of the $(200)_\alpha$ diffraction reflection was measured. The dependence of β on the depth of the treated layer was studied for LT in the modes of autoquenching and melting. A nonmonotonic change of β was observed in both cases. In the case of surface melting, the value of β was less (Fig. 21, curve *2*).

The second term in Eq. (7) can be determined from the expression [80, 81]

$$\sigma^{II}_{0.2} = \frac{MaGb}{\sqrt{\rho}}, \qquad (9)$$

where M is the Taylor multiplier (equal to 3.05 for the b.c.c. lattice), a is a constant equal to 0.11, G is the lattice shear modulus of α-Fe (85 GPa), b denotes the Burgers vector modulus (equal to $2.48 \cdot 10^{-10}$ m), and ρ is the dislocation density.

The value of ρ is calculated from the physical broadening of the $(200)_\alpha$ diffraction line according to Ref. [82] from the expression

$$\rho = \frac{\beta^2 \mathrm{ctg}^2\theta}{b^2 N f(\upsilon, h, k, l)}; \qquad (10)$$

here, β is the physical widening of the diffraction line, θ is the Bragg angle, logarithmic function

$$N = \ln\left[\frac{1}{\sqrt{\pi a}} C_\upsilon \ln\left(\frac{1}{\sqrt{\pi a}} C_\upsilon\right)\right]$$

with $a = 0.11$, $C_\upsilon = 5.5$, and the function $f(\upsilon, h, k, l) = (1 - \Gamma)/3$ relates to

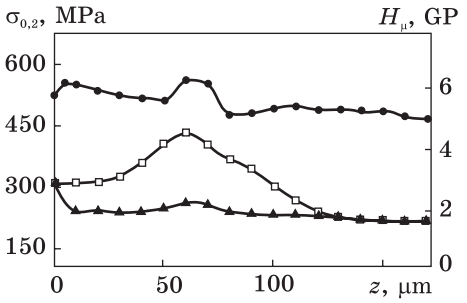

Fig. 23. Change in the yield strength $\sigma_{0.2}$ (*1*) and microhardness H_μ measured on the sample end (*2*) and after layer-by-layer etching (*3*) of the Armco iron over the depth of LIZ [90]

the crystallographic orientation and elastic properties of dislocations, where

$$\Gamma = \frac{(h^2k^2 + k^2l^2 + l^2h^2)}{(h^2 + k^2 + l^2)^2}.$$

The density of dislocations in the LIZ of Armco iron was in the range of 3×10^9–$5\cdot10^{10}$ cm^{-2}, which is consistent with the study of carbonyl iron foils irradiated in a pulsed mode [38]. The density of dislocations achieved at LT is commensurate with their concentration in the deformed material after high compression ratios. With an increase in the carbon content in steel, the dislocation density after laser quenching increases.

Taking into account the calculated density of dislocations, we obtain the component of the yield strength $\sigma^{II}_{0.2}$ equal to 250–350 MPa, which is by 1.47–2.0 times greater than the initial value of the yield strength of Armco iron (Fig. 22, curve *2*). Therefore, after laser melting, the yield strength of Armco iron is of 460–650 MPa, *i.e.*, increased by a factor of 2.7–3.7 compared to the yield strength of the initial sample, and the increase due to an increase in the dislocation density turned out to be large (Fig. 23, curve *1*). The regularities of change of $\sigma_{0.2}$ over the depth of the layer treated with continuous laser radiation, apparently, may be different due to the higher cooling rate in the case of pulsed radiation. This can lead to both the formation of a qualitatively different fine-grained structure and the appearance of a different pattern of residual stresses.

It should be noted that the above values are conditional. The results of the corresponding calculations should be considered only as an attempt to qualitatively assess the ability of near-surface layers to flow. Apparently, the conclusion about the nonmonotonic change in the yield characteristics with depth can be useful in the analysis of the exploitation sustainability of steel details under mechanical loads with a significant tangential component. In particular, such regularity of change can lead to a slowdown in the wear process at a certain degree of wear of the detail.

The increase in $\sigma_{0.2}$ can be compared with the value of strengthening achieved as a result of dissolution of carbon in an iron-based α-solid solution or strengthening of metastable iron–nickel alloys as a result of phase hardening from γ–α–γ-transformations [83].

As shown in Ref. [84], the LT of AISI 1045 steel in the quenching mode did not improve its mechanical properties. At the same time, LT with subsequent tempering or surface melting somewhat increased the mechanical properties of AISI 1045 steel. In this case, the yield strength increased to 1040 MPa after LT and subsequent tempering, *i.e.*, increases only by 1.3 times. In laser strengthening of steel, all three hardening factors contribute. Therefore, it can be concluded that the effect of laser strengthening of technical iron and low-carbon steels is more significant. With LT high-carbon and alloyed steels, the effect of strengthening is already less.

An increase in $\sigma_{0.2}$ of Armco iron correlated with an increase in the microhardness of the strengthened layer. The microhardness was measured both in the plane of the strengthened layer after each etching and along the end face of the sample. In both cases, the microhardness had a maximum value at a depth of 60–70 μm, and the microhardness measured along the end of the section (Fig. 23, curve *2*) had a greater value than after etching (Fig. 23, curve *3*).

The formation of microhardness after LT is largely affected by internal stresses, which arise, when the crystal lattice is distorted due to thermal shock. Apparently, layer-by-layer etching reduces the effect of internal stresses. Therefore, by subtracting the microhardness values obtained after etching from the total values obtained at the end of the section, it is possible to estimate the contribution of internal stresses to the formation of the mechanical properties of Armco iron after LT.

It should be noted that the magnitude of distortions and the concentration of defects in materials subjected to laser irradiation and the action of a shock (explosive) pulse turn out to be of the same order. This suggests that the elastic wave, regardless of whether it arises due to a strong temperature gradient during LT or due to a mechanical impulse, is the cause of structure fragmentation, an increase in the dislocation density and the level of lattice distortions.

7. Regularities of Residual Stresses Formation in the Armco-Fe and Steels

During pulse LT, there is an uneven distribution of temperatures over the LIZ, as a result of which the residual stresses (σ_{res}) are characterised by high gradients. Most of the works are concerned with the study of the distribution of residual stresses over the depth of the LIZ. Practical interest is the distribution in the near-surface layer of a detail treated with laser radiation, since the magnitude and sign of residual stresses have a significant effect on its strength, wear resistance, corrosion resistance, fatigue strength and other physical and mechanical properties.

LT was performed by pulsed radiation with pulse energy of 3–10 J. X-ray investigation of the samples was carried out on a Dron-3 diffrac-

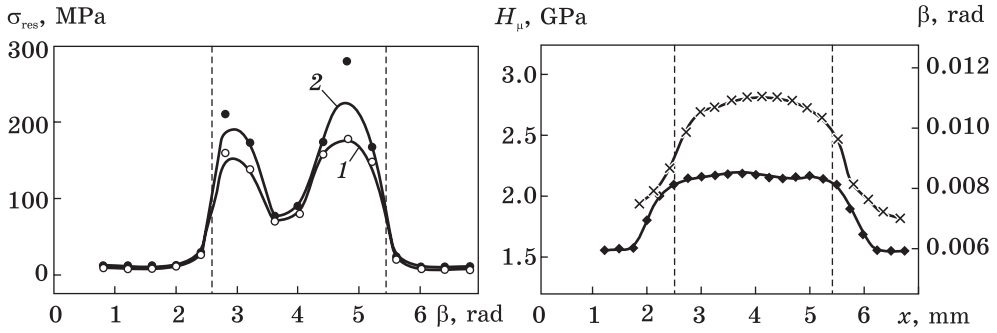

Fig. 24. Distribution of residual stresses σ_{res} over the width x of the laser track in the Armco iron after LT. W_E = 2.2 J/mm² (*1*) and 2.9 J/mm² (*2*). Dashed lines indicate the edges of the laser track [85]

Fig. 25. The change of microhardness H_μ (*1*) and physical broadening β of the $(211)_\alpha$ (*2*) reflex over the width x of the laser track in the Armco iron after LT (W_E = = 2.9 J/mm²) [85]

tometer, and residual stresses were measured using the $\sin^2\psi$ method [85]. The distribution of the width of the laser track is formed by mutual overlapping (10–20%) of laser spots.

The results of the experimental determination on the surface of Armco iron are shown in Fig. 24 [86, 87]. The dependence turned out to be close to symmetric with respect to the middle of the laser track. During LT without surface melting with an energy density of 2–2.9 J/mm², insignificant tensile stresses (≈70 MPa) were observed in the centre of the laser track, which increased to 230–270 MPa from the centre of the laser track to the boundary of the LIZ–unirradiated metal and gradually decreased to the initial value (≈20 MPa) in non-irradiated areas. In the case of LT without melting with a lower energy ($W_E \approx 2.2$ J/mm²), the character of the distribution was retained, but with a more symmetrical dependence and smaller peaks in the amplitude values. The microhardness H_μ in this LT mode increased slightly (Fig. 25, curve *1*), reaching a value of 2.1 GPa (the initial value of Armco iron is of 1.5–1.6 GPa), and practically did not change along the width of the laser track in the irradiated zone. A noticeable change in the microhardness values of Armco iron with an increase in the laser radiation energy for the LT mode without melting was not observed. The value of the physical broadening β of the $(211)_\alpha$ reflex increased over the entire width of the laser path (Fig. 25, curve *2*), indicating an increase in the dislocation density in the near-surface layers. Changes in the crystal lattice parameter a_α were not observed.

As a result of LT with surface melting (W_E = 10.2 J/mm²), there was a change in the character of the distribution (Fig. 26). In the centre of the laser track, stresses changed their sign and became compressive, reaching a value of ≈250 MPa. The maximal compressive stresses were observed in

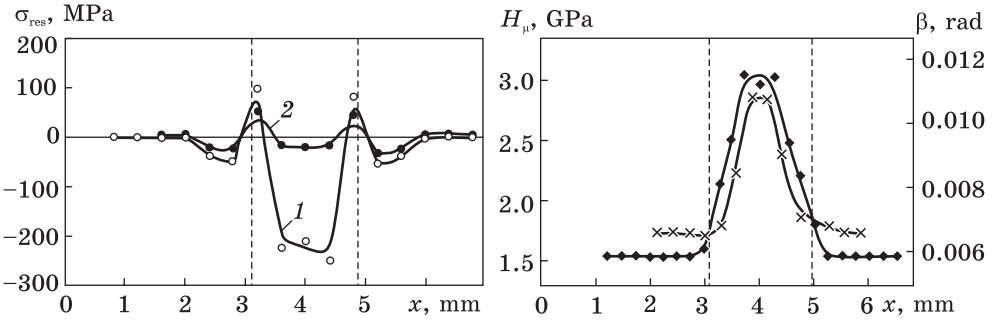

Fig. 26. Distribution of residual stresses σ_{res} over the width x of the laser track in the Armco Fe after LT. W_E = 10.2 J/mm² (*1*), 14.2 J/mm² (*2*) [51]

Fig. 27. The change of microhardness H_μ (*1*) and physical broadening β of the $(211)_\alpha$ (*2*) reflex over the width x of laser track in the Armco iron after LT (W_E = 10.2 J/mm²) [59]

the local areas with martensitic structure. At the transition boundary of the melt–initial matrix, an abrupt change in the character of stresses was observed. In these areas, peaks of tensile stresses were formed, the values of which reached 100 MPa. With an increase in the radiation energy (W_E = 14.2 J/mm²), the character of the distribution over the width of the laser track was retained, but with smaller differences in values of σ_{rest}. Under different LT modes with a change in the width of the laser track, there was also a change in the width of the tensile stress zone.

The microhardness H_μ at LT with melting changed with a pronounced maximum in the centre of the laser track (Fig. 27, curve *1*). The dependence of the physical widening (β) of the $(211)_\alpha$ reflex had an appropriate character (Fig. 27, curve 2).

During LT without melting of the surface of AISI 1035 and AISI 1045 steels (W_E = 2.9 J/mm²), no significant increase in microhardness was observed along the width of the laser track (Fig. 28). At the same time, residual tensile stresses (up to 430 MPa) were formed on the surface of the laser track, caused by plastic shortening deformations.

During LT with surface melting (W_E = 14.2 J/mm²), a martensitic transformation occurred in the treatment zone at the cooling stage, causing the appearance of residual compressive stresses. In the central melted part of the track on the surface of AISI 1035 and AISI 1045 steels, the compressive stresses increased to −200 MPa (Fig. 29). This can be associated with the geometric features of the laser dimple, *i.e.*, with the formation of a crater in the centre of the laser spot. A significant broadening of the $(211)_\alpha$ reflection may also indicate the possibility of enriching the central part of the laser spot with carbon due to its upward diffusion into the crater zone.

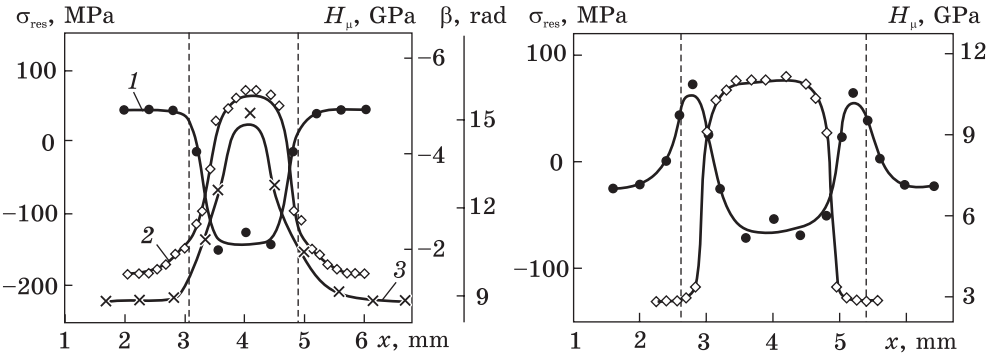

Fig. 28. Distribution of residual stresses σ_{res} (*1*), change of microhardness H_μ (2) and physical broadening β of the $(211)_\alpha$ (*3*) over the width of laser track *x* in the AISI 1035 steel after LT [86]

Fig. 29. Distribution of residual stresses σ_{res} (*1*) and change of microhardness H_μ (2) over the width of laser track *x* of the AISI W1 steel after LT. W_E = 2.9 J/mm² [16]

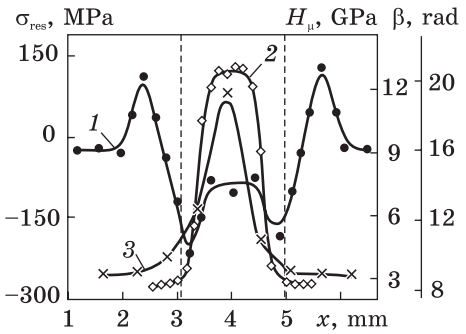

Fig. 30. Distribution of residual stresses σ_{res} (*1*), change of microhardness H_μ (*2*) and physical broadening β of the $(211)_\alpha$ (*3*) over the width of laser track *x* of the AISI W110 steel after LT. W_E = 14.2 J/mm² [86]

The character of the change in stresses depending on the LT modes was also preserved during irradiation of AISI W110 steel (Fig. 30), but with somewhat smaller drops in amplitude stress values than in AISI 1035 steel.

As shown in Ref. [20], the magnitude and sign of stresses are determined both by the LT regimes and by the initial structural and phase composition of the steel. In the case of LT with melting of steel, residual compressive stresses were formed in the near-surface layers and in the case of LT without melting, tensile stresses were formed. When the surface melted, an increase in the level of compressive stresses was observed in the central part of the LIZ. At the same time, the tensile stresses in the transition regions from the LIZ to the initial steel structure decreased with a gradual transition to compressive stresses.

The distribution of residual stresses (RS) during LT is also significantly affected by the velocity of the laser beam over the sample surface [88–90]. At a low speed (≈8 mm/s), tensile stresses up to 140 MPa were formed in the centre of the laser track after melting of AISI 1045 and

AISI 5140 H steels, and significant compressive stresses (–440 MPa) appeared along the edges of the track. With an increase in the velocity of movement, the stresses in the centre of the track change from tensile to compressive. For AISI W1 steel, the dependence of the character of distribution of residual stresses on the change in the velocity of the laser beam is insignificant [90].

As shown in Ref. [90], the magnitude and character of the distribution of residual stresses change significantly during treatment with overlapping of laser tracks. The distribution of stresses on the surface of an AISI 5140 H steel bar across hardened tracks deposited on the surface in a spiral by a continuous CO_2-laser with overlapping turns was studied. On the surface of the first six tracks, tensile stresses were revealed, and, on the last two tracks, compressive ones were revealed.

Thus, despite the significant unevenness in the character of the distribution of residual stresses in the near-surface layers of iron and steels, after pulsed LT, the presented results allow us to make conclusions about the most general regularities of their formation [85, 87–90].

The character of the distribution of RS depends on the LT modes and the carbon content in the steel. The value and sign of s_{rest} depend on the ratio of residual plastic deformations caused by local thermal action, volumetric effects of structural transformations and melt surface saturation by embodiment atoms processes. The character of the distribution of RS on the surface of the laser impact zone is symmetrical with respect to the centre of the spot and depends on the energy distribution in the laser beam. A large temperature gradient between the melt and the matrix, which is characteristic of LT, leads to the formation of tensile stress peaks. The character of the change in tensile RS caused by plastic shortening deformations correlates with the dependence of changes in microhardness and physical broadening of reflections. The accumulation of tensile RS in the volume of the metal contributes to the initiation and development of microcracks.

The occurrence of compressive RS is typical for LT with surface melting. In this case, their distribution over the LIZ is a nonmonotonic dependence that correlates with changes in microhardness, physical broadening of reflections, and the crystal lattice parameter. Compressive RS are formed in the case of the formation of a sufficient amount of martensite in the central part of the laser track during the LT process at the stage of cooling. A decrease in the amount of martensite during LT of steel leads to a decrease in the volume effect during cooling and, accordingly, to a decrease in compressive RS. Their value depends on the degree of overheating of the metal during LT in the γ-region and the cooling rate at the stage of γ–α-transformation. The more local LT corresponds to the higher the heating–cooling rate and, accordingly, the compressive-stress values.

8. Conclusions

To study the structural and phase state of metastable iron-based alloys treated by laser beam, the method of x-ray investigation of single-crystal samples was used, based on the use of crystallographic dependence of the orientations of the crystal lattices of the austenite and martensitic phases (the Kurdjumov–Lysak method). X-ray study of single-crystal samples made it possible to observe subtle diffraction effects, measure a small quantity of phase components, and study crystallographic orientation aspects of the structural state of γ- and α-solid solutions. During the laser melting of α-Fe single crystals, its complex recrystallization was observed, as a result of which a polycrystalline component of α-Fe was formed with a crystal lattice parameter that corresponded to the initial one, and, during melting in a narrow range of energy densities, the formation of single-crystal regions of the γ-phase with an increased lattice parameter was also observed. The reason for the fixation of the γ-phase after LT is the saturation of the γ-solid solution with nitrogen from the atmosphere and carbon from cementite particles. Therefore, the γ-phase observed in this work should be considered residual austenite of the Fe–N–C system, and not a γ-modification of pure α-iron. Due to the high cooling-rate characteristic of the pulsed LT, a significant textural discrepancy in the relative intensity of the γ-phase reflexes was observed. The formation of a polycrystalline structure after laser melting led to such a texture, in which the axes of easy magnetisation of a large number of crystals are mutually parallel due to their orientation mainly in the direction of heat removal. This, in turn, leads to the emergence of a magneto-crystallographic preferred direction and an increase in the saturation magnetisation of α-iron.

The implementation of resonance conditions at LT with pulses of millisecond duration led to the formation of instability of the melt surface with the formation of a wavy morphology during subsequent crystallisation. An interval of intercritical values of the energy density was established, in which instability and the nature of the change in the number of surface waves with increasing radiation energy were manifested. Based on electron microscopy studies, it is shown that, under pulsed LT conditions, a nonmonotonic dependence of dislocation density on depth emerges, accompanied by the formation of a spectrum of structures within a single laser spot. During laser melting of α-Fe, the yield strength of the hardened layer increased by more than three times that is compared to hardening from phase hardening or deformation hardening with high degrees of compression. The increase in the yield strength was mainly determined by the increase in the density of dislocations and the grinding of the structure, and the first factor is stronger. With the depth of the processed layer, the yield strength and microhardness changed according to nonmonotonic curves with a maximum. The characteristics of fluidity and microhardness in the near-surface layers of steels after LT changed according to corre-

lated curves with a maximum, and an increase in the carbon content led to a blurring of the extremum, and an increase in the energy of laser radiation to its displacement towards deeper layers. The specified strong properties were determined by such structural factors as the density of dislocations and dispersion of the structure, of which the first factor was stronger. The character of the distribution of residual stresses on the surface of LIZ is symmetrical with respect to the centre of the spot and depends on the distribution of energy in the laser beam. A significant temperature gradient between the melt and the matrix, which is characteristic of a pulsed LT, leads to the formation of peaks of tensile stresses, and with increasing cooling speed, the value of these stresses increases. The emergence of residual compressive stresses is characteristic of LT with surface melting, and their distribution over the surface of the LIZ is a nonmonotonic dependence, which correlates with the maximum of microhardness and physical broadening of reflexes.

The presented results make it possible to expand and supplement the existing ideas about the nature of the structural state of low-carbon steels formed under the conditions of high-speed laser heating. The revealed regularities of the formation of residual austenite, laser hardening due to structural factors, and distribution of residual stresses can be used in practice in the development of new intensive methods for improving the complex of physical and mechanical properties of local areas of the near-surface layers of steels and related materials [91–93].

Authors' Contributions. First author (V.Yu.D.): problem statement, justification, and conclusions. Second author (V.I.B.): sections 1–3, 7, 8. Third author (Ye.M.D.): sections 4–6, 8; figures and references.

REFERENCES

1. Z. Li, J. Chen, X. Wang, X. Shen, Y. Cen, J. Chen, Y. Chu, and Y. Han, *Mater. Sci. Eng. A*, **850**: 142568 (2022); https://doi.org/10.1016/j.msea.2022.143568
2. H.J. Breukelman, M.J. Santofimia, and J. Hidalgo, *Mater. Des.*, **221**: 110984 (2022); https://doi.org/10.1016/j.matdes.2022.110984
3. B. Syed, P. Maurya, S. Lenka, G. Padmanabham, and S.M. Shariff, *Opt. Laser Technol.*, **143**: 107285 (2021); https://doi.org/10.1016/j.optlastec.2021.107285
4. M. Probstle, S. Neumeier, J. Hopfenmuller, L.P. Freund, T. Niendorf, D. Schwarze, and M. Goken, *Mater. Sci. Eng. A*, **674**: 299 (2016); https://doi.org/10.1016/j.msea.2016.07.061
5. L.N. Carter, C. Martin, P.J. Withers, and M.M. Attallah, *J. Alloys Compd.*, **615**: 338 (2014); https://doi.org/10.1016/j.jallcom.2014.06.172
6. B. Baufeld, E. Brandl, and O. Van der Biest. *J. Mater. Process. Technol.*, **211**: 1146 (2011); https://doi.org/10.1016/j.jmatprotec.2011.01.018
7. L. Rickenbacher, S. Hovel, and K. Wegener. *Rapid Prototyping J.*, **19**, No. 4: 282 (2013); https://doi.org/10.1108/13552541311323281

8. J.Y. Natoli, L. Gallais, H. Akhouayri, and C. Amra, *Appl. Opt.*, **41**, No. 16: 3156 (2002); https://doi.org/10.1364/AO.41.003156
9. T. Niendorf, S. Leuders, A. Riemer, H. Richard, T. Troster, and D. Schwarze, *Metallurg. Mater. Trans. B*, **44**, No. 4: 794 (2013); https://doi.org/10.1007/s11663-013-9875-z
10. L.C. Ardila, F. Garciandia, J.B. Gonzalez–Diaz, P. Alvarez, A. Echeverria, M.M. Petite, R. Deffley, and J. Ochoa, *Physics Procedia*, **56**: 99 (2014); https://doi.org/10.1016/j.phpro.2014.08.152
11. J. Suryawanshi, K.G. Prashanth, and U. Ramamurty, *J. Alloys Compd.*, **725**: 355 (2017); https://doi.org/10.1016/j.jallcom.2017.07.177
12. M. Mehrpouya, A. Gisario, and M. Elahinia, *J. Manuf. Process.*, **31**: 162 (2018); https://doi.org/10.1016/j.jmapro.2017.11.011
13. C. Donik, A. Kocijan, I. Paulin, M. Hocevar, P. Gregorcic, and M. Godec, *Appl. Surf. Sci.*, **453**: 383 (2018); https://doi.org/10.1016/j.apsusc.2018.05.066
14. J. Fiocchi, C.A. Biffi, S. Gambaro, C. Paternoster, D. Mantovani, and A. Tuissi, *J. Mater. Res. Technol.*, **9**, No. 6: 13474 (2020); https://doi.org/10.1016/j.jmrt.2020.09.104
15. K. Kunze, T. Etter, J. Grasslin, and V. Shklover, *Mater. Sci. Eng. A*, **620**: 213 (2015); https://doi.org/10.1016/j.msea.2014.10.003
16. B. Polchuk, *Vliyanie Lazernoi Impulsnoi Obrabotki na Strukturno-Fazovoe Sostoyanie Pripoverkhnostnykh Sloev Splavov na Osnove Zheleza* [Effect of Laser Pulsed Treatment on Structure and Phase State of the Near-Surface Layers of Iron-Based Alloys] (Thesis of Disser. for Dr. Phys.-Math. Sci.) (Kiev: G.V. Kurdyumov Institute for Metal Physics, N.A.S.U.: 1999) (in Russian).
17. V. Danilchenko, V. Sagaradze, Ph. L'Heritier, and V. Shabashov, *Mater. Sci. Eng. A*, **357**: 146 (2002); https://doi.org/10.1016/S0921-5093(02)00023-0
18. V. Danilchenko, V. Sagaradze, Ph. L'Heritier, and I. Sagaradze, *J. Phys. IY: L, France*, **112**: 441 (2003); https://doi.org/10.1051/jp4:2003920
19. V. Danilchenko and Y. Sidorin, *Mater. Sci. Forum*, **228**: 563 (1996); https://doi.org/10.4028/www.scientific.net/MSF.228-231.563
20. A. Grigorjanc, A. Safonov, and V. Majorov, *Met. Sci. Treat. Met.*, No. 9: 45 (1987) (in Russian).
21. D. Mirzaev, *Kinetika, Struktura i Termodinamicheskie Zakonomernosti Fazovykh Prevrashchenij v 3d-Metallakh i Ikh Splavakh* [Kinetic, Structure, and Thermodynamic Regularities of Phase Transformations in 3*d*-Metals and Their Alloys] (Thesis of Disser. for Dr. Phys.-Math. Sci.) (Sverdlovsk: Sverdlovsk Institute of Metal Physics, R.A.S.: 1989) (in Russian).
22. V. Danilchenko, D. Anpilogov, and V. Girzon, *Metals*, **5**: 97 (1997).
23. V. Danilchenko, V. Bondar, and Yu. Sidorin, *Phys. Met. Metallogr.*, **74**, No. 5: 498 (1992).
24. V. Danilchenko, V. Bondar, and Ie. Dzevin, *Appl. Nanosci.*, **10**: 4625 (2020); https://doi.org/10.1007/s13204-020-01403-0
25. A. Vol, *Struktura i Svoistva Dvoinikovykh Sistem* [Structure and Properties of Twinned Systems] (Moskva: Gos. Izd. Phys.-Math. Lit.: 1982) (in Russian).
26. I. Zolotarevskiy, *Magnitnyye Svoistva GTsK-Fazy Splavov Zheleza v Oblasti Paraprotsessa i Martensitnoye GTsK–OTsK Prevrashchenie v Silnykh Impulsnykh*

Magnitnykh Polyakh [Magnetic Properties of F.C.C. Phase of Iron Alloys in the Paraprocess Region and Martensitic F.C.C.–B.C.C. Transformation in Strong Pulse Magnetic Fields] (Thesis of Disser. for Dr. Phys.-Math. Sci.) (Donetsk State University: 1991) (in Russian).
27. V. Burdin, V. Gridnev, V. Minakova, V. Trefilov, and S. Firstov, *Obrazovanie Promezhutochnoi Fazy pri* $\alpha \leftrightarrow \gamma$ *Prevrashchenii v Zheleze i Uglerodistykh Stalyakh* [Formation of Middle Phase at the $\alpha \leftrightarrow \gamma$ Transformation in Iron and Carbon Steels] (Kiev: Naukova Dumka: 1979) (in Russian).
28. K. Chuistov, M. Tomashevskiy, and A. Perekos, *Metallofizika*, **12**, No. 5: 59 (1990) (in Russian).
29. V. Elutin, I. Blinkov, and A. Ivanov, *DAN USSR*, **316**, No. 6: 1393 (1991) (in Russian).
30. E. Colombo, G. Fratucello, and F. Ronconi, *J. Magn. Magn. Matter.*, **66**: 331 (1987); https://doi.org/10.1016/0304-8853(87)90166-1
31. C.L. Fu and A. Freeman. *Phys. Rev. B*, **35**, No. 3: 925 (1987); https://doi.org/10.1103/PhysRevB.35.925
32. P. Montano and W. Gayanath, *Phys. Rev. Lett.*, **59**, No. 97: 1041 (1987); https://doi.org/10.1103/PhysRevLett.59.1041
33. H. Yamashita, M. Yoshikawa, and C. Funabiki. *J. Magn. Magn. Matter.*, **62**, No. 2: 726 (1987); https://doi.org/10.1063/1.339753
34. N. Rykalin and A. Uglov, *Surf. Phys. Chem. Mech.*, No. 6: 5 (1983) (in Russian).
35. A. Brovko, L. Mikhailova, and A. Romanova, *Metallofiz. Noveishie Tekhnol.*, No. 1: 77 (1991) (in Russian).
36. L. Golovko, *Tekhnologichni Osnovy Keruvannya Yakistyu Poverkhnevogo Sharu pry Laserniy Zmitsnyuyuchiy Obrobtsi Materialiv* [Thechnologycal Base of the Regulating of the Quality of Surface Layer by Laser Hardening Treatment of the Materials] (Thesis of Disser. for Dr. Phys.-Math. Sci.) (Kyiv: Kyiv Polytechnic Institute: 1994) (in Ukrainian).
37. Ia. Golovchiner, R. Landa, and L. Halin, *Izluchenie Mozaichnoi Struktury Gamma-Fazy Zhelezo–Nikelevykh Splavov pri Priamom i Obratnom Martensitnom Prevrashchenii* [Studying the Mosaic Structure of Gamma-Phase of Fe–Ni Alloys at the Direct and Reverse Martensitic Transformation] (Moskva: Metallurgizdat: 1958) (in Russian).
38. G. Borodina, V. Kraposhin, Yu. Romanov, and F. Kosyrev, *Met. Sci. Treat. Met.*, No. 4: 14 (1983) (in Russian).
39. V. Kraposhin, K. Shahlevitch, and T. Viazmina, *Met. Sci. Treat. Met.*, No. 10: 21 (1989) (in Russian).
40. S. Gorelik, L. Rastorguev, and Yu. Skakov, *Rentgenograficheskiy i Ehlektronnoopticheskiy Analiz* [X-Ray and Electron Analysis] (Moskva: Metallurgiya: 1970) (in Russian).
41. V. Schastlivtsev, D. Mirzaev, and I. Iakovleva, *Struktura Termicheski Obrabotannoi Stali* [Structure of the Thermotreated Steel] (Moskva: Metallurgiya: 1994) (in Russian).
42. S. Fedosov, *Phys. Chem. Mater. Treat.*, No. 1: 92 (1992) (in Russian).
43. P. Molian, *J. Mater. Sci.*, **20**, No. 8: 2903 (1985); https://doi.org/10.1007/BF00553054
44. T. Bell and W. Owen, *J. Iron Steel Instruments*, No. 4: 428 (1967).
45. S. Kous, D. Sun, and Y. Le, *Met. Trans. A*, **14A**: 643 (1983); https://doi.org/10.1007/BF02643780
46. A. Uglov and A. Galiev, *Phys. Chem. Mater. Treat.*, No. 4: 10 (1981); https://doi.org/10.1070/QE1980v010n02ABEH009908

47. A. Galiev, L. Krapivin, L. Mirkin, and A. Uglov, *DAN USSR*, **251**, No. 2: 336 (1980) (in Russian).
48. V. Ilinskiy, A. Zukov, L. Kostylev, and V. Loktyushin, *Metalls*, No. 3: 46 (1998) (in Russian).
49. V. Lakomskiy and G. Torkhov, *DAN USSR*, **183**, No. 1: 87 (1968) (in Russian).
50. V. Danilchenko, V. Bondar, and B. Polchuk, *Phys. Met. Metallogr.*, **84**, No. 4: 449 (1997).
51. V. Danilchenko, V. Bondar, and B. Polchuk, *Mater. Sci. Forum*, **321–324**, 595 (2000); https://doi.org/10.4028/www.scientific.net/MSF.321-324.595
52. V. Danilchenko, P. Volosevitch, and B. Polchuk, *Phys. Met. Metallogr.*, **91**, No. 6: 590 (2001).
53. V. Danilchenko and B. Polchuk, *Mater. Sci. Forum*, **378–381**: 440 (2001); https://doi.org/10.4028/www.scientific.net/MSF.378-381.440
54. G. Izmailov and V. Gorbach, *DAN USSR*, **286**, No. 2: 348 (1986) (in Russian).
55. G. Vasserman and I. Greven, *Tekstura Metallicheskikh Materialov* [Texture of the Metallic Materials] (Moskva: Metallurgiya: 1969) (Russian translation).
56. O. Kolerov, A. Logvinov, and A. Ryasnyi, *Phys. Chem. Mater. Treat.*, No. 1: 98 (1997) (in Russian).
57. Yu. Dragoshanskiy and B. Sokolov, *Izv. AN USSR*, **53**, No. 4: 610 (1989) (in Russian).
58. I. Popova, G. Brashevan, V. Divinskiy, L. Medvedovskaya, and S. Fedorova, *Izv. AN USSR*, **53**, No. 4: 636 (1989) (in Russian).
59. V. Danilchenko and B. Polchuk, *Met. Sci. Treat. Met.*, **1**: 3 (2000).
60. V. Danilchenko and B. Polchuk, *Met. Sci. Treat. Met.*, **2**: 15 (2001).
61. L. Lysak, Yu. Polischuk, and Ia. Vovk, *Zavodskaya Laboratoriya*, No. 4: 1021 (1968) (in Russian).
62. V.N. Bugayev, V.G. Gavrilyuk, V.M. Nadutov, and V.A. Tatarenko, *Fizika Metallov i Metallovedenie*, **68**, No. 5: 931 (1989) (in Russian); idem, *Physics of Metals and Metallography*, **68**, No. 5: 931 (1989).
63. V.A. Tatarenko and C.L. Tsynman, *Solid State Ionics*, **101–103**: 1061 (1997); https://doi.org/10.1016/s0167-2738(97)00376-7
64. V.A. Tatarenko and T.M. Radchenko, *Usp. Fiz. Met.*, **3**, No. 2: 111 (2002) (in Ukrainian); https://doi.org/10.15407/ufm.03.02.111
65. T.M. Radchenko, V.A. Tatarenko, and S.M. Bokoch, *Metallofiz. Noveishie Tekhnol.*, **28**, No. 12: 1699 (2006); https://doi.org/10.48550/arXiv.1406.0147
66. T.M. Radchenko and V.A. Tatarenko, *Defect Diffus. Forum*, **273–276**: 525 (2008); https://doi.org/10.4028/www.scientific.net/DDF.273-276.525
67. V.A. Tatarenko, S.M. Bokoch, V.M. Nadutov, T.M. Radchenko, and Y.B. Park, *Defect Diffus. Forum*, **280–281**: 29 (2008); https://doi.org/10.4028/www.scientific.net/DDF.280-281.29
68. T.M. Radchenko, O.S. Gatsenko, V.V. Lizunov, and V.A. Tatarenko, *Prog. Phys. Met.*, **21**, No. 4: 580 (2020); https://doi.org/10.15407/ufm.21.04.580
69. Ye. Levchenko and A. Chernyakov, *Zh. Eksp. Teor. Fiz.*, **81**, No. 1: 202 (1981) (in Russian).
70. L. Landau and E. Lifshitz, *Mekhanika Sploshnykh Sred* [Mechanics of Solid Environments] (Moskva: Gostekhizdat: 1953) (in Russian).
71. A. Vedenov and G. Gladush, *Fizicheskie Protsessy pri Lazernoi Obrabotke Materialov* [Physical Processes at the Laser Treatment of Materials] (Moskva: Ehnergoatomizdat: 1985) (in Russian).

72. S. Anisimov, S. Goldberg, O. Kulikov, N. Pilipetskiy, and M. Tribelskiy, *Pisma v Zh. Tekh. Fiz.*, **9**, No. 4: 226 (1983) (in Russian).
73. B. Zyryakov, A. Fannibo, and N. Yuryshev, *Phys. Chem. Mater. Treat.*, No. 3: 14 (1970) (in Russian).
74. N. Rykalin, A. Uglov, and A. Kokora, *Phys. Chem. Mater. Treat.*, No. 6: 14 (1972) (in Russian).
75. A. Grigoryants, V. Gavrilyuk, and A. Misyurov, *Teoreticheskie Osnovy Lazernoi Tekhniki* [Technical Basis of the Laser Technics] (Moskva: MVTU: 1987) (in Russian).
76. I. Zuev, S. Selishchev, and V. Skobelkin, *DAN USSR*, **254**, No. 6: 1326 (1980) (in Russian).
77. B. Chalmers, *Teoriya Zatverdevaniya* [Theory of Solidification] (Moskva: Metallurgiya: 1968) (Russian translation).
78. V. Sadovskiy, V. Schastlivtsev, T. Tabatchikova, and I. Iakovleva, *Lazernyi Nagrev i Struktura Stali: Atlas Mikrostruktur* [Laser Heating and Structure of Steel: Microstructures] (Sverdlovsk: UrO AN USSR: 1989) (in Russian).
79. D. Gureev, *Phys. Chem. Mater. Treat.*, No. 1: 27 (1994) (in Russian).
80. G. Chin and W. Mamme, *Trans. Metall. Soc. AIME*, **239**, No. 9: 1400 (1967).
81. R. Nabarro, Z. Basinsia, and D. Holt, *Adv. Phys.*, **13**, No. 50: 193 (1964); https://doi.org/10.1080/00018736400101031
82. M. Krivoglaz, *Difraktsiya Rentgenovskikh Luchei i Neitronov v Idealnykh Kristallah* [Diffraction of the X-Rays and Neutrons in the Perfect Crystals] (Kiev: Naukova Dumka: 1983) (in Russian).
83. A. Malyshev, V. Sagaradze, and I. Sorokin, *Fazovyi Naklep Austenitnykh Stalei na Zhelezo-Nikelevoi Osnove* [Phase Hardening of the Iron–Nickel-Based Austenitic Steels] (Moskva: Nauka: 1982) (in Russian).
84. D. Vasiliev and V. Trofimov, *Zavodskaya Laboratoriya*, No. 2: 20 (1984) (in Russian).
85. V. Danilchenko and B. Polchuk, *Phys. Met. Metallogr.*, **95**, No. 5: 103 (2001) (in Russian).
86. V. Danilchenko and B. Polchuk, *Mater. Sci, Forum*, **378–381**: 443 (2001); https://doi.org/10.4028/www.scientific.net/MSF.378-381.443
87. V. Danilchenko, V. Bondar, and B. Polchuk, *Metallofiz. Noveishie Tekhnol.*, **23**: 254 (2001) (in Russian).
88. D. Gureev, *Phys. Chem. Mater. Treat.*, No. 1: 31 (1993) (in Russian).
89. A. Grigoryants and A. Safonov, *Lazernaya Tekhnika i Tekhnologiya* [Laser Technics and Technology] (Moskva: Vysshaya Shkola: 1988) (in Russian).
90. V. Danilchenko, V. Bondar, and B. Polchuk, *Mater. Sci. Forum*, **378–381**, 440 (2001); https://doi.org/10.4028/www.scientific.net/MSF.378-381.440
91. O.V. Movchan and K.O. Chornoivanenko, *Prog. Phys. Met.*, **24**, No. 3: 446 (2023); https://doi.org/10.15407/ufm.24.03.446
92. M.G. Bolotov, G.P. Bolotov, and M.M. Rudenko, *Prog. Phys. Met.*, **25**, No. 1: 74 (2024); https://doi.org/10.15407/ufm.25.01.074
93. V.O. Burlakov and O.V. Filatov, *Prog. Phys. Met.*, **26**, No. 4: 968 (2025); https://doi.org/10.15407/ufm.26.04.968

Received / Final version
10.09.2025 / 22.07.2026

В.Ю. Данільченко, В.Й. Бондар, Є.М. Дзевін
Інститут металофізики ім. Г.В. Курдюмова НАН України,
бульв. Академіка Вернадського, 36, 03142 Київ, Україна

СТИМУЛЬОВАНІ ЛАЗЕРОМ СТРУКТУРНІ ТА ФАЗОВІ ПЕРЕТВОРЕННЯ У ПРИПОВЕРХНЕВИХ ШАРАХ СПЛАВІВ НА ОСНОВІ ЗАЛІЗА

Розглянуто й проаналізовано результати досліджень формування структурного стану моно- та полікристалів заліза і сплавів на його основі у різко нерівноважних умовах імпульсного лазерного оброблення. Показано, що високі швидкості нагрівання–охолодження під час лазерного оброблення спричиняють зниження температури γ–α-перетворення й утворення γ-фази. За таких умов відбувається перекристалізація монокристалів α-заліза, внаслідок чого формується полікристалічна складова α-заліза з параметром ОЦК-ґратки, який відповідає вихідному, а під час топлення у вузькому інтервалі густин енергії також формується монокристалічна область γ-фази зі збільшеним параметром ГЦК-ґратки та значною текстурою. Встановлено, що механічні властивості за глибиною зони лазерного впливу визначаються переважно структурними чинниками та змінюються за немонотонними кривими з максимумом. Виявлено вплив енергетичних параметрів імпульсного лазерного опромінення на формування хвилястої мікрогеометрії поверхні.

Ключові слова: лазерне оброблення, монокристал α-заліза, структура, аустеніт, мартенсит, залишкові напруження.